Nigerian Journal of Theoretical and Environmental Physics (NJTEP)
ISSN Print: 3026-9601
DOI: https://doi.org/10.62292/njtep.v3i2.2025.79
Volume 3(2), June 2025

Determination of Thermodynamic Properties via Partition Function Approaches Derived from the Non-Relativistic Schrödinger Equation

***[1]Peter J. Manga., [1]Ramoni O. Amusat, [1]Peter B. Teru, [1]Amina A. Dibal, [1]Wana E. Likta, [2]Oyelade V. Omolara, [3]Adamu Z. Ngari, [4]Dauda S. Buteh, [5]Nuhu S. Gin and [6]Sheik A. Ubale**

[1]Department of Physics, University of Maiduguri, Borno State – Nigeria.
[2]Department of Physics, Bingham University, Karu, Nasarawa State – Nigeria
[3]Department of Physics, Nigeria Army University Biu, Borno State - Nigeria
[4]Department of Chemistry, Adamu Tafawa Balewa College of Education, Kangere, Bauchi State – Nigeria.
[5]Department of Chemistry, Federal University of Gashua, Yobe State – Nigeria.
[6]Department of Fine and Applied Art, Aminu Saleh College of Education Azare, Bauchi State – Nigeria.

*Corresponding author's email: 2016peterjohn@gmail.com

ABSTRACT

A critical challenge in molecular thermodynamics is accurately predicting how variations in dimensionless potential parameters influence macroscopic properties such as magnetisation, specific heat capacity, and molecular vibrational entropy. Traditional approaches often fail to fully capture these dependencies, limiting their predictive accuracy. In this study, we address this gap by developing a rigorous framework based on partition function formulations derived directly from the non-relativistic Schrödinger equation. Our main aim is to investigate the impact of dimensionless potential parameters (V_0 and V_1) and the temperature parameter (β) on energy spectrum and key thermodynamic and magnetic properties. We systematically compute the energy spectrum for a wide range of potential parameter values and analyse their effects on magnetisation, magnetic susceptibility, internal energy, free energy, entropy, and specific heat capacity. The findings reveal that energy spectrum exhibit strong dependence on these parameters, with V_0 generally reducing energy levels while V_1 enhances them. Magnetisation typically decreases with V_0 but increases with V_1 and higher temperatures, while magnetic susceptibility shows complex patterns of enhancement and suppression. Vibrational thermodynamic properties, including internal energy and free energy, also display significant variations tied to the interplay of potential parameters. This study provides a robust, first-principles-based method for understanding and predicting how microscopic potential parameters govern macroscopic thermodynamic behaviour, advancing the fundamental knowledge and practical capabilities of molecular thermodynamics.

Keywords:
Dimensionless Potential Parameter,
Magnetisation,
Magnetic Susceptibility,
Partition Function,
Specific Heat Capacity.

INTRODUCTION

Understanding and forecasting thermodynamic properties is essential across disciplines like chemical engineering, materials science, energy physics and molecular physics. Key properties—including internal energy, entropy, free energy, and heat capacity—provide valuable information about the stability, chemical reactivity, and equilibrium characteristics of molecular systems (Abu-shady *et al.*, 2023). Statistical mechanics offers one of the most robust and informative frameworks for evaluating these macroscopic properties, effectively linking quantum-level behaviour with observable large-scale phenomena (Abu-shady *et al.*, 2023).

Central to this approach is the partition function, a key element in statistical mechanics. It encapsulates how energy states are statistically distributed in a system and forms the basis for deriving all thermodynamic properties (Abu-shady *et al.*, 2023). To compute the partition function, one must understand the energy levels of the system—information typically acquired for molecular systems by solving the Schrödinger equation, a core principle of quantum mechanics that governs the

evolution of quantum states over time (Abu-shady *et al.*, 2023).

Specifically, the non-relativistic Schrödinger equation is often employed to model molecular systems in cases where relativistic effects are insignificant. Solving this equation yields the permissible energy levels of the system, which are essential for building the partition function. With the partition function determined, numerous thermodynamic properties can be derived through standard mathematical formulations (Manga *et al.*, 2023).

This method—referred to as partition function modelling grounded in quantum mechanics—enables the prediction of thermodynamic behaviour from first principles (Onate *et al*., 2022). It is particularly advantageous for analysing isolated molecules, gases, and other systems where quantum effects are prominent (Mulian, 2025). Additionally, it facilitates predictions independent of experimental data, making it highly beneficial for both theoretical research and practical applications such as reaction kinetics, phase equilibrium analysis, and the design of new materials (Ding *et al.*, 2011).

Within this framework, the current research emphasizes the evaluation of thermodynamic properties through partition function models based on the non-relativistic Schrödinger equation. By examining both the theoretical foundations and computational methods, this study seeks to highlight the efficiency and relevance of this quantum-statistical approach in contemporary thermodynamic investigations.

2. Hylleraas plus Yukawa Potential (Modified Hylleraas Potential (MHsP))

The study of both relativistic and non-relativistic solutions to wave equations within quantum mechanical systems has gained increasing global interest (Umirzakov, 2019). Over the past decade, numerous researchers have developed mathematical frameworks to solve the Schrödinger equation, focusing on deriving both the energy spectrum and corresponding wavefunctions (Dong, 2000). These solutions have been applied across a wide range of physical systems. In this work, we utilize the Modified Hylleraas Potential (MHp), which allows for exact solutions with relatively low mathematical complexity (Reiss, 1980). Originally introduced to model intermolecular interactions, the Hylleraas potential has been shown to be well-suited for multi-particle systems and vibrational energy analyses of diatomic molecules. According to Ikot *et al.*, (2021), the Hylleraas potential exhibits a multi-exponential parameter structure, yet limited research has explored its bound state solutions within both relativistic and non-relativistic quantum systems. To further extend its applicability, a variant known as the Modified Hylleraas plus Yukawa Potential (MHsP) has also been proposed for similar investigations (Manga *et al*., 2021).

$$V(r) = \frac{V_0}{b}\frac{a- e^{-2\beta r}}{1- e^{-2\beta r}} + \frac{V_1\, e^{-2\beta r}}{r} \qquad (1)$$

Here, β represents the potential screening parameter. Since the introduction of this potential by Hylleraas, various modifications have been suggested; however, this study concentrates specifically on the form given in equation (1). It is worth noting that only a limited number of researchers have explored or applied this potential since its initial proposal.

Radial Solution of the Schrödinger equation based on Hylleraas plus Yukawa potential (MHsP)

The radial motion of a particle under a spherically symmetric potential $V(r)$ is described by the following expression (Ikot *et al.*, 2021: Lublinsky *et al.*, 2017)

$$\frac{d^2R}{dr^2} + \left[\frac{2\mu}{\hbar^2}\big(E - V(r)\big) - \frac{\eth}{r^2}\right]R(r) = 0 \qquad (2)$$

Where $\eth = \tau(\tau+1)$ equation (2) becomes

$$\frac{d^2R}{dr^2} + \left[\frac{2\mu}{\hbar^2}\big(E - V(r)\big) - \frac{\tau(\tau+1)}{r^2}\right]R(r) = 0 \qquad (3)$$

Analytical solutions to Equation (3) are not feasible when $\tau \neq 0$ due to the complexity introduced by the centrifugal term (Manga *et al.*, 2021). To address this, we employ the Greene and Aldrich approximation method for the centrifugal term as outlined Edet *et al.*, 2023).

$$\frac{1}{r^2} = \frac{4\delta^2 e^{-2\delta r}}{\left(1-e^{-2\delta r}\right)^2} = \frac{1}{r} = \frac{2\delta e^{-2\delta r}}{(1-e^{-2\delta r})} \qquad (4)$$

It is important to note that for short-range potentials, Equation (4) serves as a reasonable approximation for $\frac{1}{r^2}$. However, this approximation becomes less accurate when the screening parameter δ is large, making it unsuitable for describing the centrifugal barrier under such conditions. The approximation remains valid only when $\delta r \ll 1$. Therefore, by substituting Equation (1) into Equation (2), and subsequently applying the Greene and Aldrich approximation as defined in Equation (4), we obtain the following expression (Edet *et al.*, 2023).

$$\frac{d^2R}{dr^2} + \left[\frac{2\mu}{\hbar^2}\left(E - \frac{V_0}{b}\frac{a- e^{-2\gamma r}}{1- e^{-2\gamma r}} + \frac{2\gamma V_1\, e^{-4\gamma r}}{(1-e^{-2\gamma r})}\right) - \frac{4\gamma^2 e^{-2\gamma r}\tau(\tau+1)}{(1-e^{-2\gamma r})^2}\right]R(r) = 0 \qquad (5)$$

The coordinate in Equation (1) is transformed as follows.

$$\frac{d^2}{dr^2} + \frac{1}{v}\frac{d}{dr} + \frac{1}{v^2(1-v)^2}\left(\frac{\mu E}{2\gamma^2\hbar^2} - \frac{\mu E v}{\gamma^2\hbar^2} + \frac{\mu E v^2}{2\gamma^2\hbar^2} - \frac{V_0 a}{4\gamma^2 b} + \frac{V_0 u}{4\gamma^2 b} + \frac{V_0 a v}{4\gamma^2 b} - \frac{V_0 v^2}{4\gamma^2 b} - \frac{V_1 v}{\gamma} + \frac{V_1 v^2}{\gamma} - v\tau^2 - v\tau\right)R(v) = 0 \qquad (6)$$

A transformation is applied to Equation (6) to facilitate obtaining its hypergeometric solution.

$$\frac{d^2}{dr^2} + \frac{1(1-v)}{v(1-v)}\frac{d}{dr} + \frac{1}{v^2(1-v)^2}\{(-C_1 - C_3 + C_4)u^2 + (-2C_1 + C_3 + C_2 - C_4 - \tau^2 - \tau)v - C_1 - C_2\} \qquad (7)$$

The following dimensionless constants, as defined in Equation (7), were used (Edet *et al.*, 2023).

$$\frac{\mu E}{2\gamma^2\hbar^2} = \mathrm{E}_{n,l} = C_1,\ C_2 = \frac{V_0 a}{4\gamma^2 b},\ C_3 = \frac{V_0}{4\gamma^2 b},\ C_4 = \frac{V_1}{\gamma}, \tag{8}$$

Equation (7) meets the criteria of a hypergeometric function in the following form (Ettah, 2021).

$$\psi_n'' + \frac{\chi_1 - \chi_2 s}{s(1-\chi_3 s)}\psi' + \frac{1}{s^2(1-\chi_3 s)^2}[-\mathfrak{T}_1 s^2 + \mathfrak{T}_2 s - \mathfrak{T}_3]\psi(s) = 0 \tag{9}$$

Comparing equation (7) and (8) we have

$$\mathfrak{T}_1 = -C_1 - C_3 + C_4;\ \mathfrak{T}_2 = -2C_1 + C_3 + C_2 - C_4 - \tau^2 - \tau;\ \mathfrak{T}_3 = -C_1 - C_2 \tag{10}$$

The Gauss hypergeometric equation can be expressed in the form (Edet *et al.*, 2023).

$$\delta = \frac{1}{2}\left((1-\gamma_1) \pm \sqrt{(1-\gamma_1)^2 + 4\mathfrak{T}_3}\right) \tag{11}$$

$$\delta^2 = -C_1 - C_2 \tag{12}$$

The coiling velocity, determined using the Nikiforov-Uvarov functional analysis method, is expressed as follows (Jia *et al.*, 2012).

$$\omega = \frac{1}{2\gamma_3}\left((\gamma_3 + \gamma_1\gamma_3 - \gamma_2) \pm \sqrt{(\gamma_3 + \gamma_1\gamma_3 - \gamma_2)^2 + 4\left(\frac{\mathfrak{T}_1}{\gamma_3} + \gamma_2\mathfrak{T}_3 - \mathfrak{T}_2\right)}\right) \tag{13}$$

$$\omega = \frac{1}{2}\left(1 + \sqrt{1 + 4(-2C_3 + 2C_4 + \tau^2 + \tau - 2C_2)}\right) \tag{14}$$

After equating equation (12) by equation (14) we deduced our bound state energy eigenvalue equation as;

$$\mathrm{E}_{n,l} = C_2 + \left(\frac{-C_3 + C_4 + C_2 - (\omega+n)^2}{2(\omega+n)}\right)^2 \tag{14}$$

Equation (15) can be rewrite by substituting the dimensionless constant as given in equation (8), we have

$$\mathrm{E}_{n,\tau} = \frac{2\gamma^2\hbar^2}{\mu}\frac{V_0 a}{4\gamma^2 b} + \frac{2\gamma^2\hbar^2}{\mu}\left(\frac{-\frac{V_0}{4\gamma^2 b} + \frac{V_1}{\gamma} + \frac{V_0 a}{4\gamma^2 b} - (\omega+n)^2}{2(\omega+n)}\right)^2 \tag{15}$$

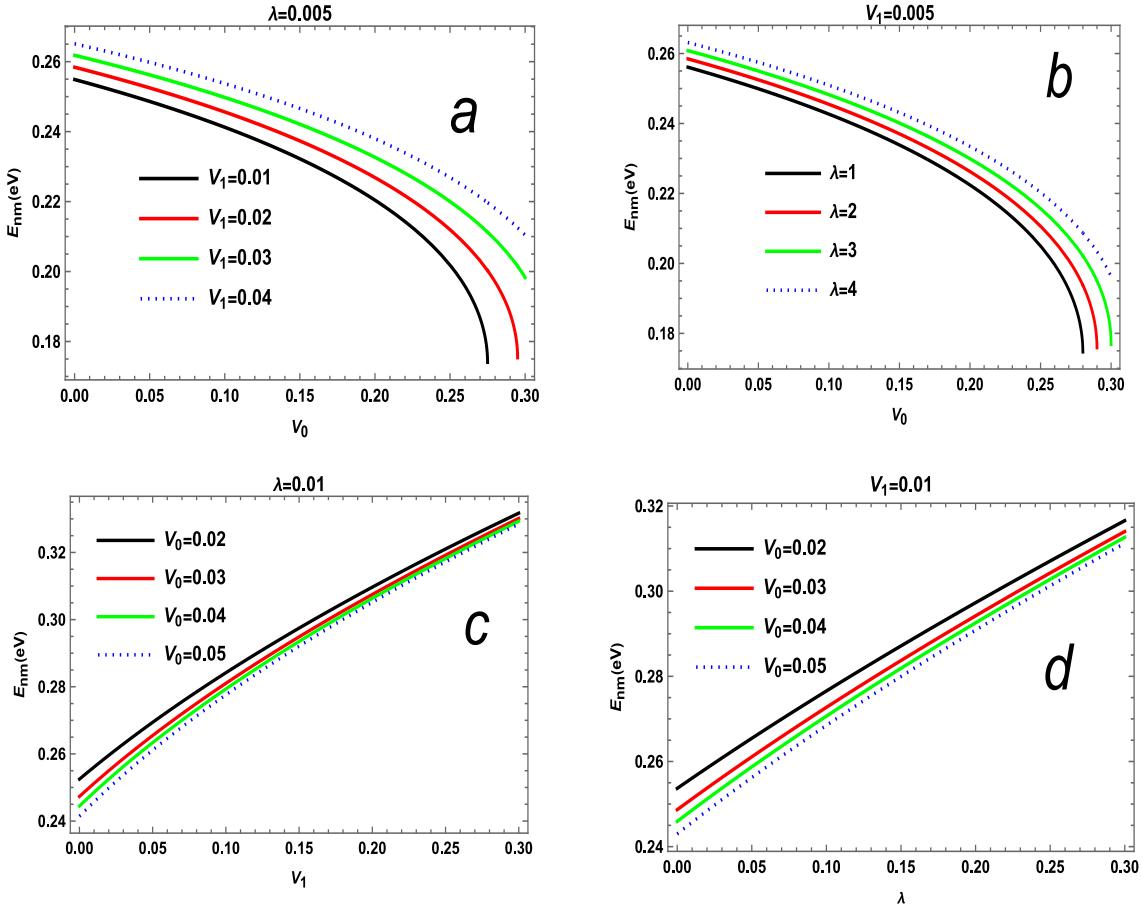

Figure 1: Computed energy spectrum under varying potential parameters

Figure 1 shows the energy spectrum computed from the non-relativistic Schrödinger equation for different dimensionless potential parameters. In subplots (a) and (b), the energy levels are higher for lower values of V_0 and V_1 with sensitivity to variations in λ and V_1 . As these parameters increase, the energy spectrum declines. A similar behaviour is observed in subplots (c) and (d), highlighting the strong dependence of energy eigenvalues on the potential parameters.

Partition function can be express as follows

$$PF = \frac{1}{2\sqrt{-k1\beta}} e^{\frac{1}{2}(-2k1k2+k2k3)\beta-\frac{1}{2}\sqrt{-k1\beta}\sqrt{k2k3^2\beta}}\sqrt{\pi}(1 + e^{\sqrt{-k1\beta}\sqrt{k2k3^2\beta}}(-1 + \mathrm{Erf}[\frac{p^2\sqrt{-k1\beta}+\sqrt{k2k3^2\beta}}{2p}]) + \mathrm{Erf}[\frac{1}{2}p\sqrt{-k1\beta} - \frac{\sqrt{k2k3^2\beta}}{2p}]) \quad (16)$$

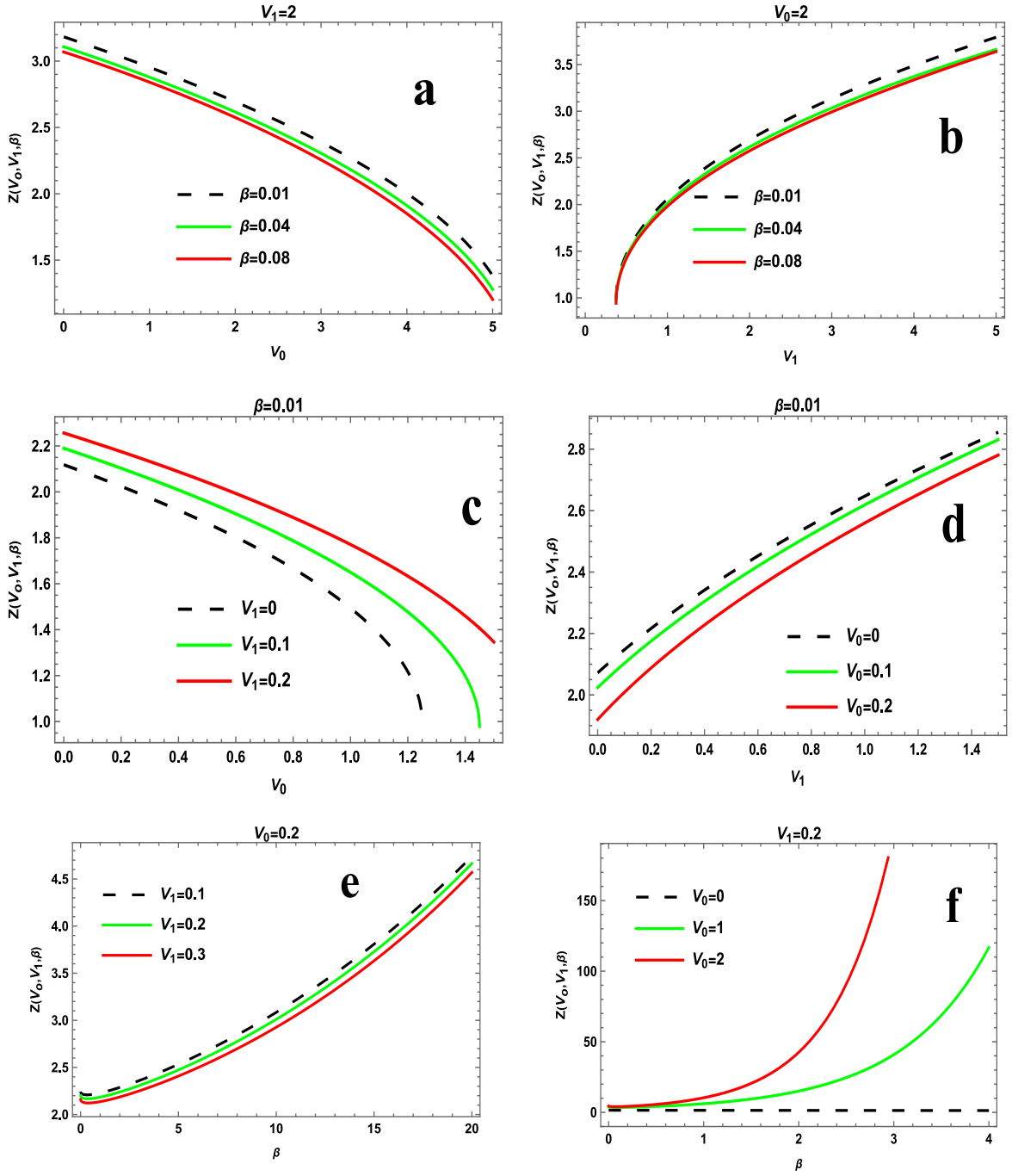

Figure 2: The plot of Partition Function Under Varying Dimensionless Potential Parameters

For figure 2; At a fixed value of λ=0.005 for the dimensionless potential parameter (Dppr), results indicate that an increase in V_0 leads to a decrease in the computed energy spectrum, whereas increasing V_1 results in higher energy levels. This suggests that raising V_1 elevates the energy spectrum. Similarly, when V_1 is held constant at 0.005, the energy spectrum decreases with increasing V_0 consistent with the trend shown in plot (a). Furthermore, at a constant V_0 a higher value of λ results in elevated energy levels, indicating that this dimensionless parameter also contributes to an increase in the energy spectrum. When λ=0.01, the energy spectrum continues to rise with increasing V_1, while larger values of V_0 cause a slight reduction in the spectrum, resulting in a downward shift of the energy curves. At a fixed $V_1 = 0.01$, the spectrum increases with λ, while higher V_0 values consistently correspond to lower energy levels across all λ values.

Magnetic magnetisation can be express as follows

$$MM = \frac{P_1(P_2\left(\frac{P_3P_4}{\sqrt{\pi}}+\frac{P_5P_6}{\sqrt{\pi}}--P_7\right)+-P_8+-P_9(P_{10}))}{P_{11}} \tag{17}$$

$$P_1 = e^{-\frac{1}{2}(-\frac{f}{8}+\frac{u}{2})\beta+\frac{1}{8}\sqrt{-f\beta}\sqrt{u^2\beta}}\sqrt{-f\beta} \tag{18}$$

$$P_2 = \frac{1}{\sqrt{-f\beta}}e^{\frac{1}{2}(-\frac{f}{8}+\frac{u}{2})\beta-\frac{1}{8}\sqrt{-f\beta}\sqrt{u^2\beta}}\sqrt{2\pi} \tag{19}$$

$$P_3 = 2e^{-(\frac{(2+\sqrt{1+4(1-f+2u)})\sqrt{-f\beta}}{8\sqrt{2}}-\frac{\sqrt{u^2\beta}}{\sqrt{2}(2+\sqrt{1+4(1-f+2u)})})^2} \tag{20}$$

$$P_4 = (-\frac{(2+\sqrt{1+4(1-f+2u)})\beta}{16\sqrt{2}\sqrt{-f\beta}}-\frac{\sqrt{-f\beta}}{4\sqrt{2}\sqrt{1+4(1-f+2u)}}-\frac{\sqrt{2}\sqrt{u^2\beta}}{\sqrt{1+4(1-f+2u)}(2+\sqrt{1+4(1-f+2u)})^2}) \tag{21}$$

$$P_5 = 2e^{\frac{1}{4}\sqrt{-f\beta}\sqrt{u^2\beta}-\frac{(\frac{(2+\sqrt{1+4(1-f+2u)})^2\sqrt{-f\beta}}{8\sqrt{2}}+\frac{\sqrt{u^2\beta}}{\sqrt{2}})^2}{(2+\sqrt{1+4(1-f+2u)})^2}} \tag{22}$$

$$P_6 = (\frac{-\frac{(2+\sqrt{1+4(1-f+2u)})^2\beta}{16\sqrt{2}\sqrt{-f\beta}}-\frac{(2+\sqrt{1+4(1-f+2u)})\sqrt{-f\beta}}{2\sqrt{2}\sqrt{1+4(1-f+2u)}}}{2+\sqrt{1+4(1-f+2u)}}+\frac{2\left(\frac{(2+\sqrt{1+4(1-f+2u)})^2\sqrt{-f\beta}}{8\sqrt{2}}+\frac{\sqrt{u^2\beta}}{\sqrt{2}}\right)}{\sqrt{1+4(1-f+2u)}\left(2+\sqrt{1+4(1-f+2u)}\right)^2}) \tag{23}$$

$$P_7 = \frac{e^{\frac{1}{4}\sqrt{-f\beta}\sqrt{u^2\beta}}\beta\sqrt{u^2\beta}(-1+\mathrm{Erf}[\frac{\frac{(2+\sqrt{1+4(1-f+2u)})^2\sqrt{-f\beta}}{8\sqrt{2}}+\frac{\sqrt{u^2\beta}}{\sqrt{2}}}{2+\sqrt{1+4(1-f+2u)}}])}{8\sqrt{-f\beta}} \tag{24}$$

$$P_8 = \frac{1}{(-f\beta)^{3/2}}e^{\frac{1}{2}(-\frac{f}{8}+\frac{u}{2})\beta-\frac{1}{8}\sqrt{-f\beta}\sqrt{u^2\beta}}\sqrt{\frac{\pi}{2}}\beta(1+e^{\frac{1}{4}\sqrt{-f\beta}\sqrt{u^2\beta}}(-1+$$

$$\mathrm{Erf}[\frac{\frac{(2+\sqrt{1+4(1-f+2u)})^2\sqrt{-f\beta}}{8\sqrt{2}}+\frac{\sqrt{u^2\beta}}{\sqrt{2}}}{2+\sqrt{1+4(1-f+2u)}}])Erf[\frac{(2+\sqrt{1+4(1-f+2u)})\sqrt{-f\beta}}{8\sqrt{2}}-\frac{\sqrt{u^2\beta}}{\sqrt{2}(2+\sqrt{1+4(1-f+2u)})}]) \tag{25}$$

$$P_9 = \frac{1}{\sqrt{-f\beta}}e^{\frac{1}{2}\left(-\frac{f}{8}+\frac{u}{2}\right)\beta-\frac{1}{8}\sqrt{-f\beta}\sqrt{u^2\beta}}\sqrt{2\pi}\left(-\frac{\beta}{16}+\frac{\beta\sqrt{u^2\beta}}{16\sqrt{-f\beta}}\right) \tag{26}$$

$$P_{10} = (1+e^{\frac{1}{4}\sqrt{-f\beta}\sqrt{u^2\beta}}(-1+\mathrm{Erf}[\frac{\frac{(2+\sqrt{1+4(1-f+2u)})^2\sqrt{-f\beta}}{8\sqrt{2}}+\frac{\sqrt{u^2\beta}}{\sqrt{2}}}{2+\sqrt{1+4(1-f+2u)}}])+\mathrm{Erf}[\frac{(2+\sqrt{1+4(1-f+2u)})\sqrt{-f\beta}}{8\sqrt{2}}-\frac{\sqrt{u^2\beta}}{\sqrt{2}(2+\sqrt{1+4(1-f+2u)})}]) \tag{27}$$

$$P_{11} = (\sqrt{2\pi}\beta(1+e^{\frac{1}{4}\sqrt{-f\beta}\sqrt{u^2\beta}}(-1+\mathrm{Erf}[\frac{\frac{(2+\sqrt{1+4(1-f+2u)})^2\sqrt{-f\beta}}{8\sqrt{2}}+\frac{\sqrt{u^2\beta}}{\sqrt{2}}}{2+\sqrt{1+4(1-f+2u)}}])+Erf[\frac{(2+\sqrt{1+4(1-f+2u)})\sqrt{-f\beta}}{8\sqrt{2}}-$$

$$\frac{\sqrt{u^2\beta}}{\sqrt{2}(2+\sqrt{1+4(1-f+2u)})}])) \tag{28}$$

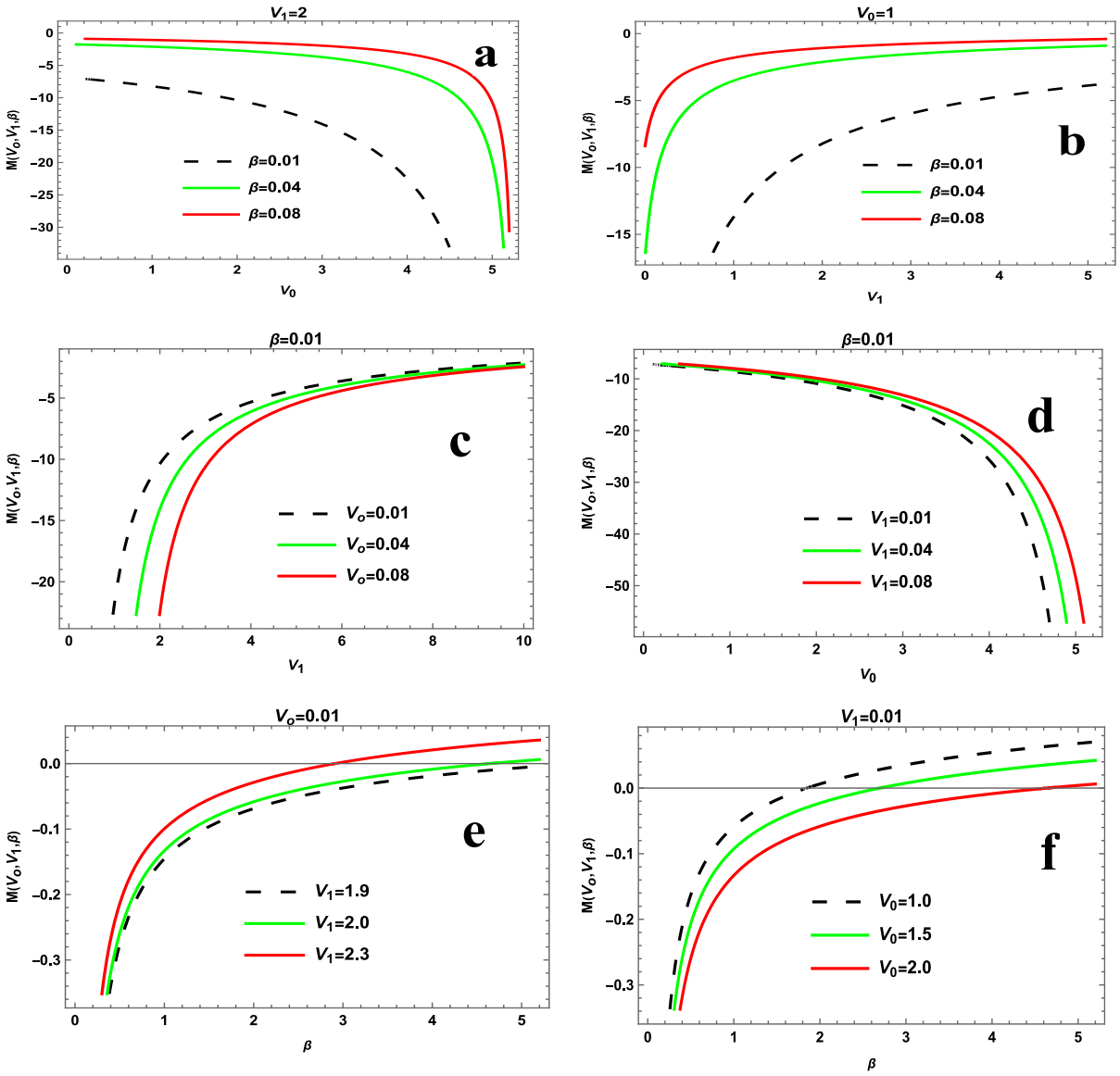

Figure 3: The plot of Magnetisation Under Varying Dimensionless Potential Parameters

Figure 3 presents the variation of magnetisation $MM(V_o, V_1, \beta)$ at finite temperatures. In Plot (a), magnetisation decreases as the dimensionless potential parameter V_o increases, particularly with rising values of the temperature-related parameter β, moving from 0.01 to 0.04. This indicates that higher thermal effects suppress magnetisation with increasing V_o. Plot (b) reveals a consistent trend where magnetisation increases as both the temperature parameter β\betaβ and the potential parameter V_1 increase.

In Plot (c), magnetisation plotted against V_1 for different values of V_0 shows a positive correlation, with magnetisation increasing as V_1 rises. Conversely, plot (d), which also plots magnetisation against V_1 but under variations in β, indicates that magnetisation decreases at higher values of V_1, suggesting a dampening effect from increased thermal activity.

Plot (e) demonstrates that a simultaneous increase in both the temperature parameter β and V_1 leads to a steady rise in magnetisation. Similarly, plot (f) shows that when magnetisation is plotted against β, there is a noticeable increase in magnetisation with rising values of both β and V_0, highlighting the combined effect of thermal and potential parameters.

Magnetic Susceptibility can be express as follows

$$X_m = \frac{\partial M}{\partial B} \qquad (29)$$

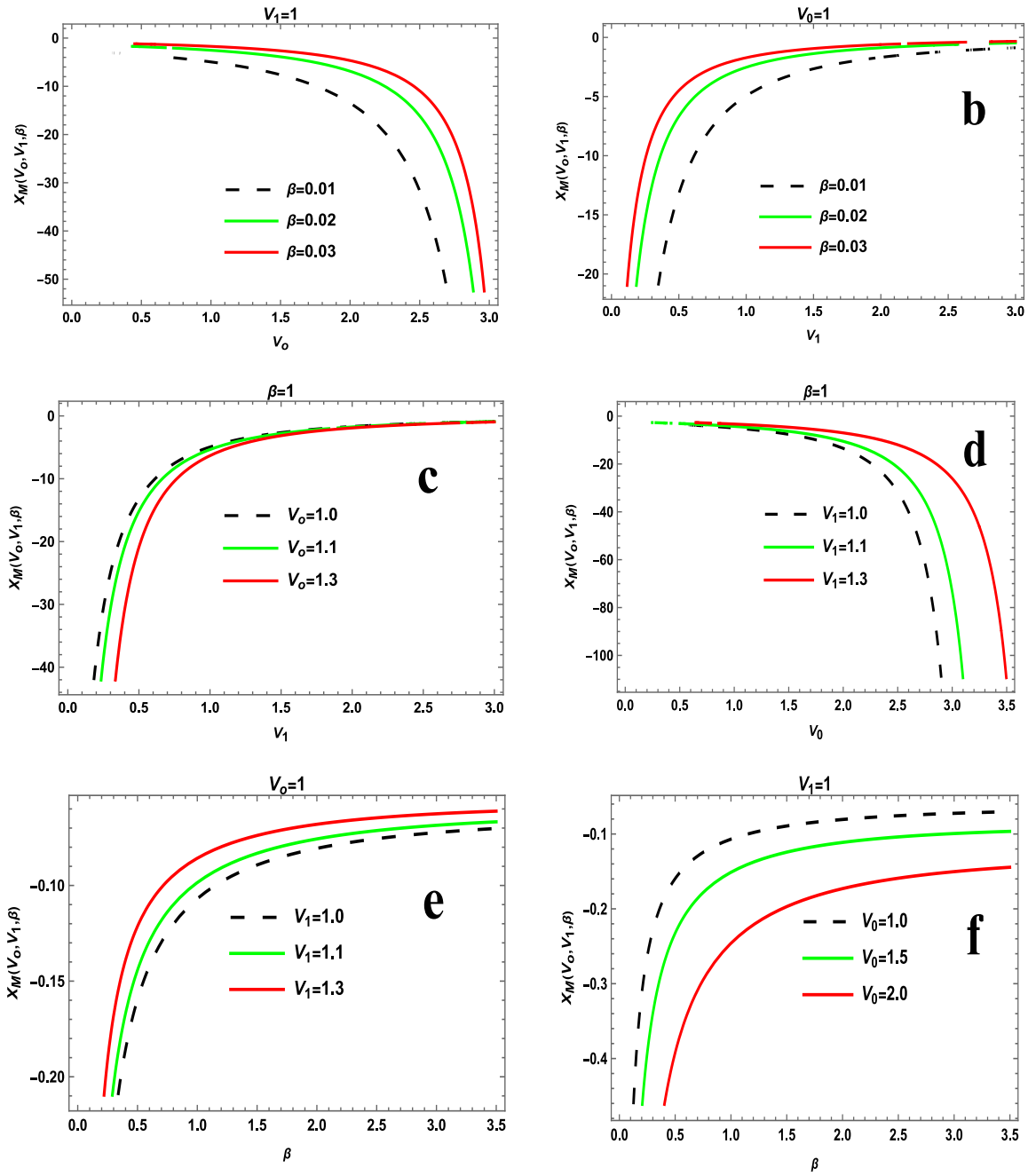

Figure 4: The plot of Magnetic Susceptibility Under Varying Dimensionless Potential Parameters

Figure 4 illustrates the behaviour of magnetic susceptibility across plots (a) to (f). In Plot (a), a decline in magnetic susceptibility is observed as both the temperature parameter and the dimensionless potential parameter increase. In contrast, plot (b) demonstrates that magnetic susceptibility rises with an increase in both the temperature parameter and the potential parameter V_1 .

Plot (c) shows a growth in magnetic susceptibility when it is plotted against V_1 , while varying the dimensionless potential parameter V_0 , indicating a positive relationship. However, in Plot (d), when both V_1 and V_0 reach higher values, a decrease in susceptibility is observed, suggesting a saturation or suppressive effect at elevated parameter levels.

Finally, Plots (e) and (f) display the variation of magnetic susceptibility with respect to the temperature parameter, under different values of V_1 and V_0 . These plots reveal that increasing the potential parameters leads to a corresponding increase in computed magnetic susceptibility.

The molecular vibrational internal energy is express as

$$U = -\frac{\partial}{\partial\beta}(LogZ) \tag{30}$$

$$U = -(\text{Log}[\beta]\Big/\text{Log}[\frac{1}{\sqrt{-\frac{af\beta\hbar^2}{b\mu}}}(-1+\text{Erf}[\frac{P_{12}+\frac{\sqrt{\beta\left(-\frac{f}{4b\delta^2}+\frac{af}{4b\delta^2}+\frac{u}{\delta}\right)^2\delta^2\hbar^2}}{\mu}}{1+n+\sqrt{1+4\left(-\frac{f}{2b\delta^2}-\frac{af}{2b\delta^2}+\frac{2u}{\delta}+\lambda\right)}}]) + P_{13} \tag{30}$$

$$P_{11} = e^{-\frac{1}{8}\sqrt{-\frac{af\beta\hbar^2}{b\mu}}\sqrt{\frac{\beta(-\frac{f}{4b\delta^2}+\frac{af}{4b\delta^2}+\frac{u}{\delta})^2\delta^2\hbar^2}{\mu}}+\frac{1}{2}\beta(\frac{(-\frac{f}{4b\delta^2}+\frac{af}{4b\delta^2}+\frac{u}{\delta})\delta^2\hbar^2}{2\mu}-\frac{af\delta^2\hbar^4}{8b\mu^2})\sqrt{2\pi}}(1+e^{\frac{1}{4}\sqrt{-\frac{af\beta\hbar^2}{b\mu}}\sqrt{\frac{\beta(-\frac{f}{4b\delta^2}+\frac{af}{4b\delta^2}+\frac{u}{\delta})^2\delta^2\hbar^2}{\mu}}}) \tag{31}$$

$$P_{12} = \frac{(1+n+\sqrt{1+4(-\frac{f}{2b\delta^2}-\frac{af}{2b\delta^2}+\frac{2u}{\delta}+\lambda)})^2\sqrt{-\frac{af\beta\hbar^2}{b\mu}}}{8\sqrt{2}} \tag{32}$$

$$P_{13} = \text{Erf}[\frac{(1+n+\sqrt{1+4(-\frac{f}{2b\delta^2}-\frac{af}{2b\delta^2}+\frac{2u}{\delta}+\lambda)})\sqrt{-\frac{af\beta\hbar^2}{b\mu}}}{8\sqrt{2}} - \frac{\sqrt{\frac{\beta(-\frac{f}{4b\delta^2}+\frac{af}{4b\delta^2}+\frac{u}{\delta})^2\delta^2\hbar^2}{\mu}}}{\sqrt{2}(1+n+\sqrt{1+4(-\frac{f}{2b\delta^2}-\frac{af}{2b\delta^2}+\frac{2u}{\delta}+\lambda)})}] \tag{33}$$

3.4 The molecular vibrational free energy can be express

$$F = \frac{1}{\beta}(LogZ) = P_{14} + P_{15} \tag{34}$$

$$P_{14} = \frac{1}{\beta}\text{Log}[\frac{1}{\sqrt{-\frac{af\beta\hbar^2}{b\mu}}}e^{-\frac{1}{8}\sqrt{-\frac{af\beta\hbar^2}{b\mu}}\sqrt{\frac{\beta(-\frac{f}{4b\delta^2}+\frac{af}{4b\delta^2}+\frac{u}{\delta})^2\delta^2\hbar^2}{\mu}}+\frac{1}{2}\beta(\frac{(-\frac{f}{4b\delta^2}+\frac{af}{4b\delta^2}+\frac{u}{\delta})\delta^2\hbar^2}{2\mu}-\frac{af\delta^2\hbar^4}{8b\mu^2})}\sqrt{2\pi} \tag{35}$$

$$P_{15} = (1+e^{\frac{1}{4}\sqrt{-\frac{af\beta\hbar^2}{b\mu}}\sqrt{\frac{\beta(-\frac{f}{4b\delta^2}+\frac{af}{4b\delta^2}+\frac{u}{\delta})^2\delta^2\hbar^2}{\mu}}}(-1+\text{Erf}[\frac{\frac{(1+n+\sqrt{1+4(-\frac{f}{2b\delta^2}-\frac{af}{2b\delta^2}+\frac{2u}{\delta}+\lambda)})^2\sqrt{-\frac{af\beta\hbar^2}{b\mu}}}{8\sqrt{2}}+\frac{\sqrt{\frac{\beta(-\frac{f}{4b\delta^2}+\frac{af}{4b\delta^2}+\frac{u}{\delta})^2\delta^2\hbar^2}{\mu}}}{\sqrt{2}}}{1+n+\sqrt{1+4(-\frac{f}{2b\delta^2}-\frac{af}{2b\delta^2}+\frac{2u}{\delta}+\lambda)}}]) \tag{36}$$

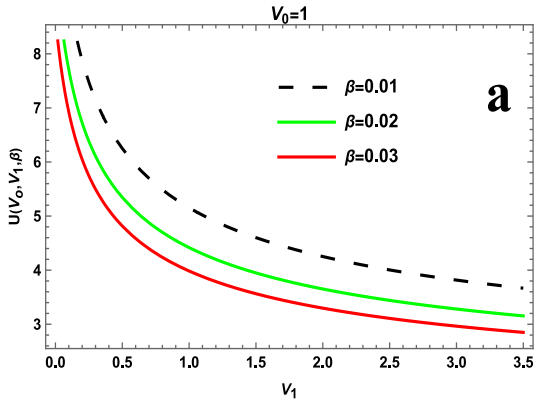

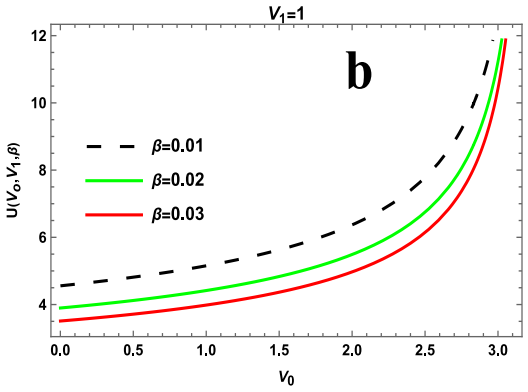

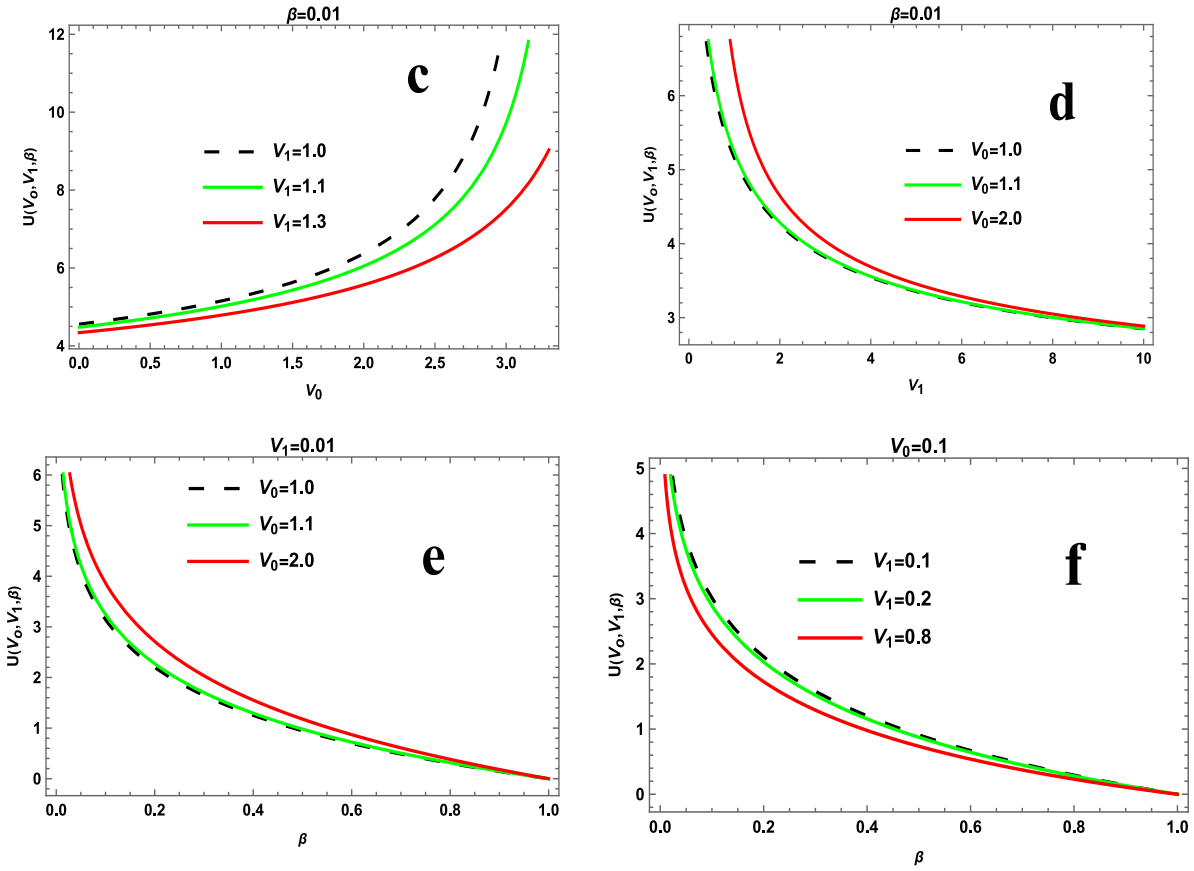

Figure 5: The Plot of Vibrational Internal Energy Under Varying Dimensionless Potential Parameters

Figure 5 illustrates the trends in molecular vibrational internal energy across several plots. In plot (a), it's observed that as both the dimensional potential parameter V_1 and the temperature parameter β increase, the molecular vibrational internal energy tends to decrease. Plot (b) shows a different behaviour: an increase in both parameters leads to a rise in molecular vibrational internal energy. Plot (c) demonstrates that the internal energy grows as both V_1 *and* V_0 increase. Conversely, plot (d) reveals that a rise in V_1 *and* V_0 leads to a decrease in molecular vibrational internal energy. Finally, plots (e) and (f) depict how variations in the temperature parameter affect the vibrational internal energy: specifically, increasing the dimensional potential parameter results in a decrease in molecular vibrational internal energy.

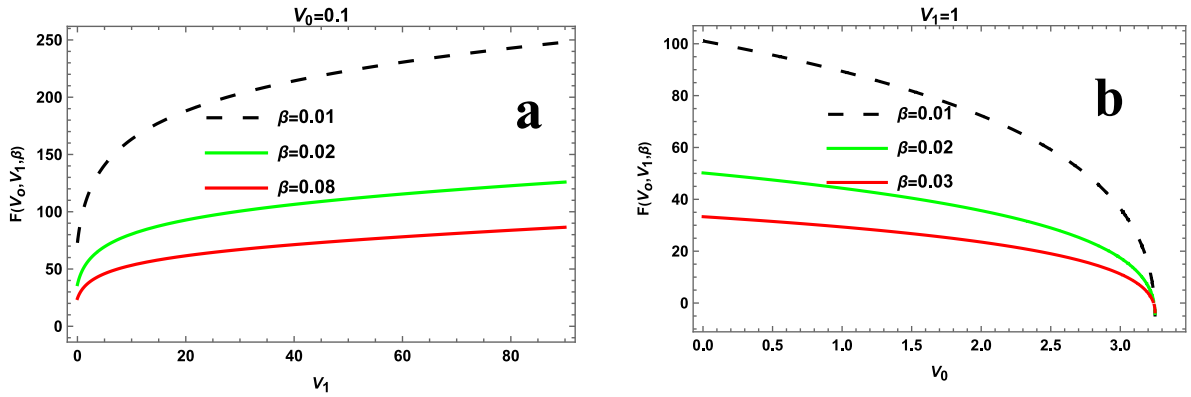

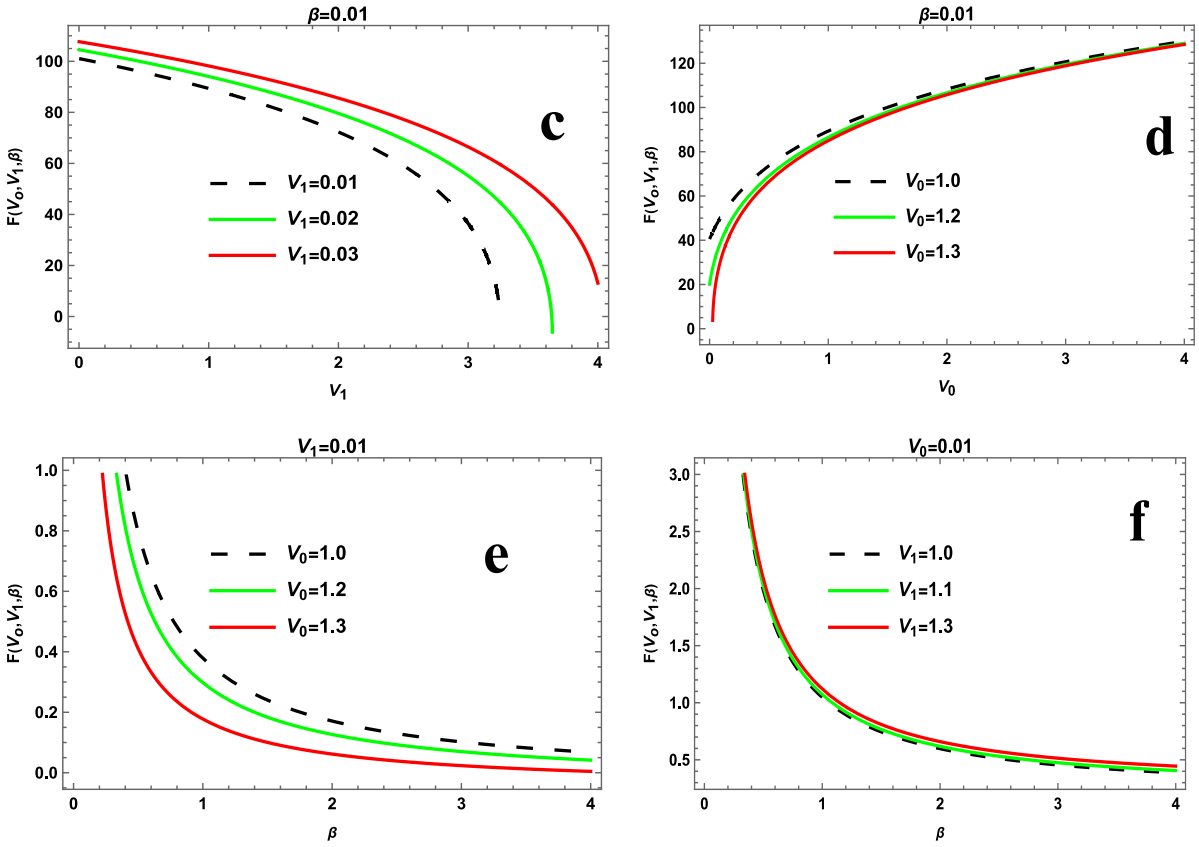

Figure 6: The plot of Vibrational Free Energy Under Varying Dimensionless Potential Parameters

Figure 6 presents the molecular vibrational free energy across different conditions. In plot (a), both the temperature parameter and the dimensionless potential parameter increase, causing the molecular vibrational free energy to rise. However, plot (b) reveals that an increase in these same parameters leads to a reduction in the molecular vibrational free energy. Plot (c) illustrates that as the dimensionless potential parameter V_1 grows, the molecular vibrational free energy decreases. In contrast, plot (d) shows that higher values of V_0 cause the molecular vibrational free energy to increase. Likewise, plots (e) and (f) demonstrate that when the temperature parameter is plotted against the molecular vibrational free energy, simultaneous increases in V_1, V_0 and the temperature parameter β result in a decline in the molecular vibrational free energy.

The molecular vibrational entropy can be express as

$$S = k_\beta \frac{\partial}{\partial \beta}(F) \tag{37}$$

$$P_{16} = \frac{\dfrac{(P_{17}P_{18}P_{19}(-\frac{af(1+n+\sqrt{1+4(-\frac{f}{2b\delta^2}-\frac{af}{2b\delta^2}+\frac{2u}{\delta}+\lambda)})^2\hbar^2}{16\sqrt{2}b\mu\sqrt{-\frac{af\beta\hbar^2}{b\mu}}}+\frac{(-\frac{f}{4b\delta^2}+\frac{af}{4b\delta^2}+\frac{u}{\delta})^2\delta^2\hbar^2}{2\sqrt{2}\mu\sqrt{\frac{\beta(-\frac{f}{4b\delta^2}+\frac{af}{4b\delta^2}+\frac{u}{\delta})^2\delta^2\hbar^2}{\mu}}}))}{(\sqrt{\pi}(1+n+\sqrt{1+4(-\frac{f}{2b\delta^2}-\frac{af}{2b\delta^2}+\frac{2u}{\delta}+\lambda)}))}+P_{20}P_{21}+P_{22}+P_{23}+P_{24}}{P_{26}}+P_{27} \tag{38}$$

$$P_{17} = e^{-\frac{1}{8}\sqrt{-\frac{af\beta\hbar^2}{b\mu}}\sqrt{\frac{\beta(-\frac{f}{4b\delta^2}+\frac{af}{4b\delta^2}+\frac{u}{\delta})^2\delta^2\hbar^2}{\mu}}+\frac{1}{2}\beta(\frac{(-\frac{f}{4b\delta^2}+\frac{af}{4b\delta^2}+\frac{u}{\delta})\delta^2\hbar^2}{2\mu}-\frac{af\delta^2\hbar^4}{8b\mu^2})}\sqrt{2\pi} \tag{39}$$

$$P_{18} = (e^{\frac{1}{8}\sqrt{-\frac{af\beta\hbar^2}{b\mu}}\sqrt{\frac{\beta(-\frac{f}{4b\delta^2}+\frac{af}{4b\delta^2}+\frac{u}{\delta})^2\delta^2\hbar^2}{\mu}}-\frac{1}{2}\beta(\frac{(-\frac{f}{4b\delta^2}+\frac{af}{4b\delta^2}+\frac{u}{\delta})\delta^2\hbar^2}{2\mu}-\frac{af\delta^2\hbar^4}{8b\mu^2})}\sqrt{-\frac{af\beta\hbar^2}{b\mu}}(\frac{1}{\sqrt{-\frac{af\beta\hbar^2}{b\mu}}} \tag{40}$$

$$P_{19} = (2e^{\frac{1}{4}\sqrt{-\frac{af\beta\hbar^2}{b\mu}}\sqrt{\frac{\beta(-\frac{f}{4b\delta^2}+\frac{af}{4b\delta^2}+\frac{u}{\delta})^2\delta^2\hbar^2}{\mu}}-\frac{(\frac{(1+n+\sqrt{1+4(-\frac{f}{2b\delta^2}-\frac{af}{2b\delta^2}+\frac{2u}{\delta}+\lambda)})^2\sqrt{-\frac{af\beta\hbar^2}{b\mu}}}{8\sqrt{2}}+\frac{\sqrt{\frac{\beta(-\frac{f}{4b\delta^2}+\frac{af}{4b\delta^2}+\frac{u}{\delta})^2\delta^2\hbar^2}{\mu}}}{\sqrt{2}})^2}{(1+n+\sqrt{1+4(-\frac{f}{2b\delta^2}-\frac{af}{2b\delta^2}+\frac{2u}{\delta}+\lambda)})^2}} \quad (41)$$

$$P_{20} = \frac{1}{\sqrt{\pi}}2e^{-\frac{(\frac{(1+n+\sqrt{1+4(-\frac{f}{2b\delta^2}-\frac{af}{2b\delta^2}+\frac{2u}{\delta}+\lambda)})\sqrt{-\frac{af\beta\hbar^2}{b\mu}}}{8\sqrt{2}}+\frac{\sqrt{\frac{\beta(-\frac{f}{4b\delta^2}+\frac{af}{4b\delta^2}+\frac{u}{\delta})^2\delta^2\hbar^2}{\mu}}}{\sqrt{2}(1+n+\sqrt{1+4(-\frac{f}{2b\delta^2}-\frac{af}{2b\delta^2}+\frac{2u}{\delta}+\lambda)})})^2}} \quad (42)$$

$$P_{21} = (-\frac{af(1+n+\sqrt{1+4(-\frac{f}{2b\delta^2}-\frac{af}{2b\delta^2}+\frac{2u}{\delta}+\lambda)})\hbar^2}{16\sqrt{2}b\mu\sqrt{-\frac{af\beta\hbar^2}{b\mu}}}-\frac{(-\frac{f}{4b\delta^2}+\frac{af}{4b\delta^2}+\frac{u}{\delta})^2\delta^2\hbar^2}{2\sqrt{2}(1+n+\sqrt{1+4(-\frac{f}{2b\delta^2}-\frac{af}{2b\delta^2}+\frac{2u}{\delta}+\lambda)})\mu\sqrt{\frac{\beta(-\frac{f}{4b\delta^2}+\frac{af}{4b\delta^2}+\frac{u}{\delta})^2\delta^2\hbar^2}{\mu}}}) \quad (43)$$

$$P_{22} = e^{\frac{1}{4}\sqrt{-\frac{af\beta\hbar^2}{b\mu}}\sqrt{\frac{\beta(-\frac{f}{4b\delta^2}+\frac{af}{4b\delta^2}+\frac{u}{\delta})^2\delta^2\hbar^2}{\mu}}}(\frac{(-\frac{f}{4b\delta^2}+\frac{af}{4b\delta^2}+\frac{u}{\delta})^2\delta^2\hbar^2\sqrt{-\frac{af\beta\hbar^2}{b\mu}}}{8\mu\sqrt{\frac{\beta(-\frac{f}{4b\delta^2}+\frac{af}{4b\delta^2}+\frac{u}{\delta})^2\delta^2\hbar^2}{\mu}}}-\frac{af\hbar^2\sqrt{\frac{\beta(-\frac{f}{4b\delta^2}+\frac{af}{4b\delta^2}+\frac{u}{\delta})^2\delta^2\hbar^2}{\mu}}}{8b\mu\sqrt{-\frac{af\beta\hbar^2}{b\mu}}})(-1+$$
$$\mathrm{Erf}[\frac{\frac{(1+n+\sqrt{1+4(-\frac{f}{2b\delta^2}-\frac{af}{2b\delta^2}+\frac{2u}{\delta}+\lambda)})^2\sqrt{-\frac{af\beta\hbar^2}{b\mu}}}{8\sqrt{2}}+\frac{\sqrt{\frac{\beta(-\frac{f}{4b\delta^2}+\frac{af}{4b\delta^2}+\frac{u}{\delta})^2\delta^2\hbar^2}{\mu}}}{\sqrt{2}}}{1+n+\sqrt{1+4(-\frac{f}{2b\delta^2}-\frac{af}{2b\delta^2}+\frac{2u}{\delta}+\lambda)}}]) \quad (44)$$

$$P_{23} = \frac{1}{b\mu(-\frac{af\beta\hbar^2}{b\mu})^{3/2}}ae^{-\frac{1}{8}\sqrt{-\frac{af\beta\hbar^2}{b\mu}}\sqrt{\frac{\beta(-\frac{f}{4b\delta^2}+\frac{af}{4b\delta^2}+\frac{u}{\delta})^2\delta^2\hbar^2}{\mu}}+\frac{1}{2}\beta(\frac{(-\frac{f}{4b\delta^2}+\frac{af}{4b\delta^2}+\frac{u}{\delta})\delta^2\hbar^2}{2\mu}-\frac{af\delta^2\hbar^4}{8b\mu^2})}f\sqrt{\frac{\pi}{2}}\hbar^2(1+$$
$$e^{\frac{1}{4}\sqrt{-\frac{af\beta\hbar^2}{b\mu}}\sqrt{\frac{\beta(-\frac{f}{4b\delta^2}+\frac{af}{4b\delta^2}+\frac{u}{\delta})^2\delta^2\hbar^2}{\mu}}}(-1+\mathrm{Erf}[\frac{\frac{(1+n+\sqrt{1+4(-\frac{f}{2b\delta^2}-\frac{af}{2b\delta^2}+\frac{2u}{\delta}+\lambda)})^2\sqrt{-\frac{af\beta\hbar^2}{b\mu}}}{8\sqrt{2}}+\frac{\sqrt{\frac{\beta(-\frac{f}{4b\delta^2}+\frac{af}{4b\delta^2}+\frac{u}{\delta})^2\delta^2\hbar^2}{\mu}}}{\sqrt{2}}}{1+n+\sqrt{1+4(-\frac{f}{2b\delta^2}-\frac{af}{2b\delta^2}+\frac{2u}{\delta}+\lambda)}}]) \quad (45)$$

$$P_{24} = P_{25}+\frac{af\hbar^2\sqrt{\frac{\beta(-\frac{f}{4b\delta^2}+\frac{af}{4b\delta^2}+\frac{u}{\delta})^2\delta^2\hbar^2}{\mu}}}{16b\mu\sqrt{-\frac{af\beta\hbar^2}{b\mu}}}+\frac{1}{2}(\frac{(-\frac{f}{4b\delta^2}+\frac{af}{4b\delta^2}+\frac{u}{\delta})\delta^2\hbar^2}{2\mu}-\frac{af\delta^2\hbar^4}{8b\mu^2}))(1+e^{\frac{1}{4}\sqrt{-\frac{af\beta\hbar^2}{b\mu}}\sqrt{\frac{\beta(-\frac{f}{4b\delta^2}+\frac{af}{4b\delta^2}+\frac{u}{\delta})^2\delta^2\hbar^2}{\mu}}}(-1+$$
$$\mathrm{Erf}[\frac{\frac{(1+n+\sqrt{1+4(-\frac{f}{2b\delta^2}-\frac{af}{2b\delta^2}+\frac{2u}{\delta}+\lambda)})^2\sqrt{-\frac{af\beta\hbar^2}{b\mu}}}{8\sqrt{2}}+\frac{\sqrt{\frac{\beta(-\frac{f}{4b\delta^2}+\frac{af}{4b\delta^2}+\frac{u}{\delta})^2\delta^2\hbar^2}{\mu}}}{\sqrt{2}}}{1+n+\sqrt{1+4(-\frac{f}{2b\delta^2}-\frac{af}{2b\delta^2}+\frac{2u}{\delta}+\lambda)}}])+\mathrm{Erf}[\frac{(1+n+\sqrt{1+4(-\frac{f}{2b\delta^2}-\frac{af}{2b\delta^2}+\frac{2u}{\delta}+\lambda)})\sqrt{-\frac{af\beta\hbar^2}{b\mu}}}{8\sqrt{2}}-$$
$$\frac{\sqrt{\frac{\beta(-\frac{f}{4b\delta^2}+\frac{af}{4b\delta^2}+\frac{u}{\delta})^2\delta^2\hbar^2}{\mu}}}{\sqrt{2}(1+n+\sqrt{1+4(-\frac{f}{2b\delta^2}-\frac{af}{2b\delta^2}+\frac{2u}{\delta}+\lambda)})}])))) \quad (46)$$

$$P_{25} = \frac{1}{\sqrt{-\frac{af\beta\hbar^2}{b\mu}}}e^{-\frac{1}{8}\sqrt{-\frac{af\beta\hbar^2}{b\mu}}\sqrt{\frac{\beta(-\frac{f}{4b\delta^2}+\frac{af}{4b\delta^2}+\frac{u}{\delta})^2\delta^2\hbar^2}{\mu}}+\frac{1}{2}\beta(\frac{(-\frac{f}{4b\delta^2}+\frac{af}{4b\delta^2}+\frac{u}{\delta})\delta^2\hbar^2}{2\mu}-\frac{af\delta^2\hbar^4}{8b\mu^2})}\sqrt{2\pi}(-\frac{(-\frac{f}{4b\delta^2}+\frac{af}{4b\delta^2}+\frac{u}{\delta})^2\delta^2\hbar^2\sqrt{-\frac{af\beta\hbar^2}{b\mu}}}{16\mu\sqrt{\frac{\beta(-\frac{f}{4b\delta^2}+\frac{af}{4b\delta^2}+\frac{u}{\delta})^2\delta^2\hbar^2}{\mu}}} \quad (47)$$

$$P_{26} = (\sqrt{2\pi}\beta(1 + e^{\frac{1}{4}\sqrt{-\frac{af\beta\hbar^2}{b\mu}}\sqrt{\frac{\beta(-\frac{f}{4b\delta^2}+\frac{af}{4b\delta^2}+\frac{u}{\delta})^2\delta^2\hbar^2}{\mu}}}(-1 + \text{Erf}[\frac{\frac{(1+n+\sqrt{1+4(-\frac{f}{2b\delta^2}-\frac{af}{2b\delta^2}+\frac{2u}{\delta}+\lambda)})^2\sqrt{-\frac{af\beta\hbar^2}{b\mu}}}{8\sqrt{2}}+\frac{\sqrt{\frac{\beta(-\frac{f}{4b\delta^2}+\frac{af}{4b\delta^2}+\frac{u}{\delta})^2\delta^2\hbar^2}{\mu}}}{\sqrt{2}}}{1+n+\sqrt{1+4(-\frac{f}{2b\delta^2}-\frac{af}{2b\delta^2}+\frac{2u}{\delta}+\lambda)}}]) + \text{Erf}[\frac{(1+n+\sqrt{1+4(-\frac{f}{2b\delta^2}-\frac{af}{2b\delta^2}+\frac{2u}{\delta}+\lambda)})\sqrt{-\frac{af\beta\hbar^2}{b\mu}}}{8\sqrt{2}} - \frac{\sqrt{\frac{\beta(-\frac{f}{4b\delta^2}+\frac{af}{4b\delta^2}+\frac{u}{\delta})^2\delta^2\hbar^2}{\mu}}}{\sqrt{2}(1+n+\sqrt{1+4(-\frac{f}{2b\delta^2}-\frac{af}{2b\delta^2}+\frac{2u}{\delta}+\lambda)})}]) \quad (48)$$

$$P_{27} = \frac{1}{\beta^2}\text{Log}[\frac{1}{\sqrt{-\frac{af\beta\hbar^2}{b\mu}}}e^{-\frac{1}{8}\sqrt{-\frac{af\beta\hbar^2}{b\mu}}\sqrt{\frac{\beta(-\frac{f}{4b\delta^2}+\frac{af}{4b\delta^2}+\frac{u}{\delta})^2\delta^2\hbar^2}{\mu}}+\frac{1}{2}\beta(\frac{(-\frac{f}{4b\delta^2}+\frac{af}{4b\delta^2}+\frac{u}{\delta})\delta^2\hbar^2}{2\mu}-\frac{af\delta^2\hbar^4}{8b\mu^2})}\sqrt{2\pi}(1 + e^{\frac{1}{4}\sqrt{-\frac{af\beta\hbar^2}{b\mu}}\sqrt{\frac{\beta(-\frac{f}{4b\delta^2}+\frac{af}{4b\delta^2}+\frac{u}{\delta})^2\delta^2\hbar^2}{\mu}}}(-1 + \text{Erf}[\frac{\frac{(1+n+\sqrt{1+4(-\frac{f}{2b\delta^2}-\frac{af}{2b\delta^2}+\frac{2u}{\delta}+\lambda)})^2\sqrt{-\frac{af\beta\hbar^2}{b\mu}}}{8\sqrt{2}}+\frac{\sqrt{\frac{\beta(-\frac{f}{4b\delta^2}+\frac{af}{4b\delta^2}+\frac{u}{\delta})^2\delta^2\hbar^2}{\mu}}}{\sqrt{2}}}{1+n+\sqrt{1+4(-\frac{f}{2b\delta^2}-\frac{af}{2b\delta^2}+\frac{2u}{\delta}+\lambda)}}]) + \text{Erf}[\frac{(1+n+\sqrt{1+4(-\frac{f}{2b\delta^2}-\frac{af}{2b\delta^2}+\frac{2u}{\delta}+\lambda)})\sqrt{-\frac{af\beta\hbar^2}{b\mu}}}{8\sqrt{2}} - \frac{\sqrt{\frac{\beta(-\frac{f}{4b\delta^2}+\frac{af}{4b\delta^2}+\frac{u}{\delta})^2\delta^2\hbar^2}{\mu}}}{\sqrt{2}(1+n+\sqrt{1+4(-\frac{f}{2b\delta^2}-\frac{af}{2b\delta^2}+\frac{2u}{\delta}+\lambda)})}])]k_\beta \quad (49)$$

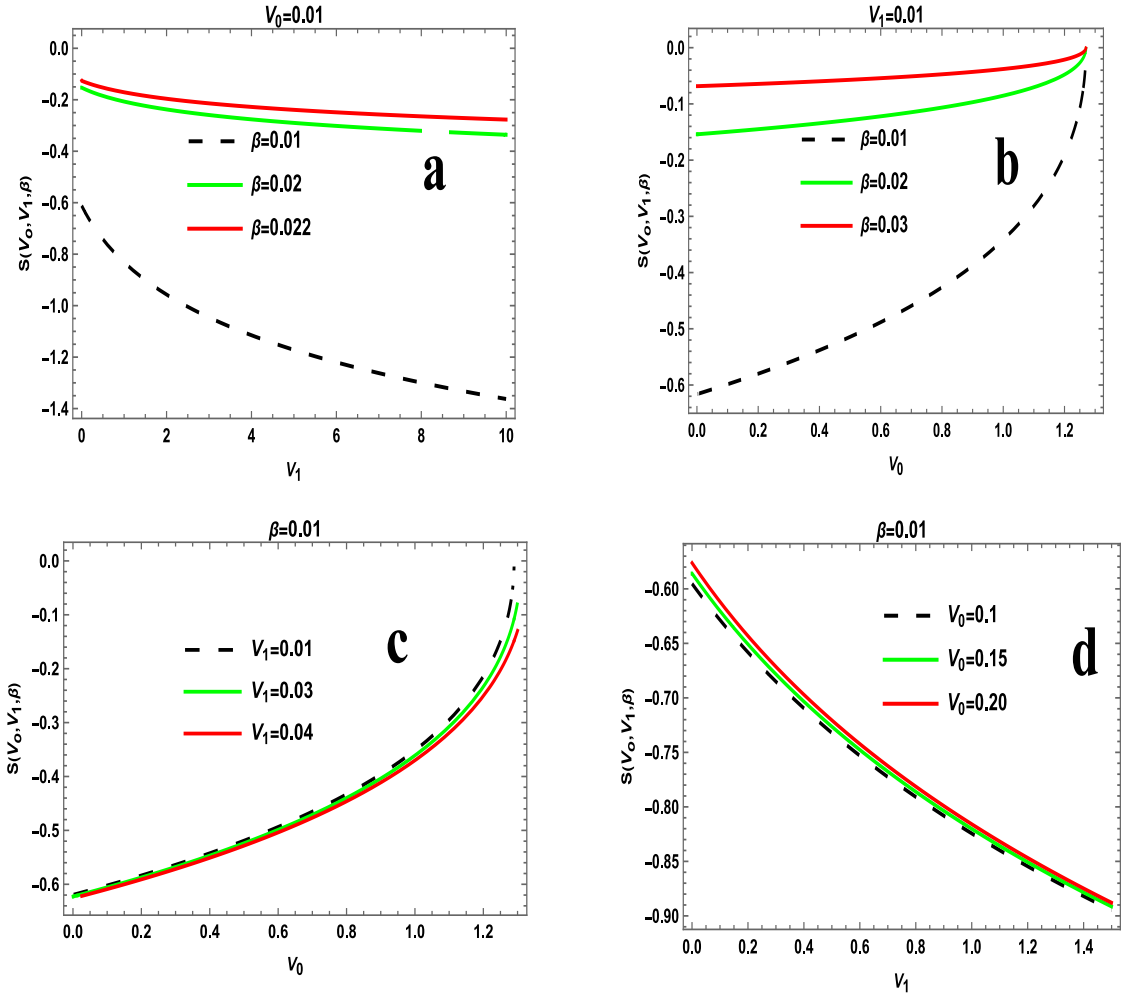

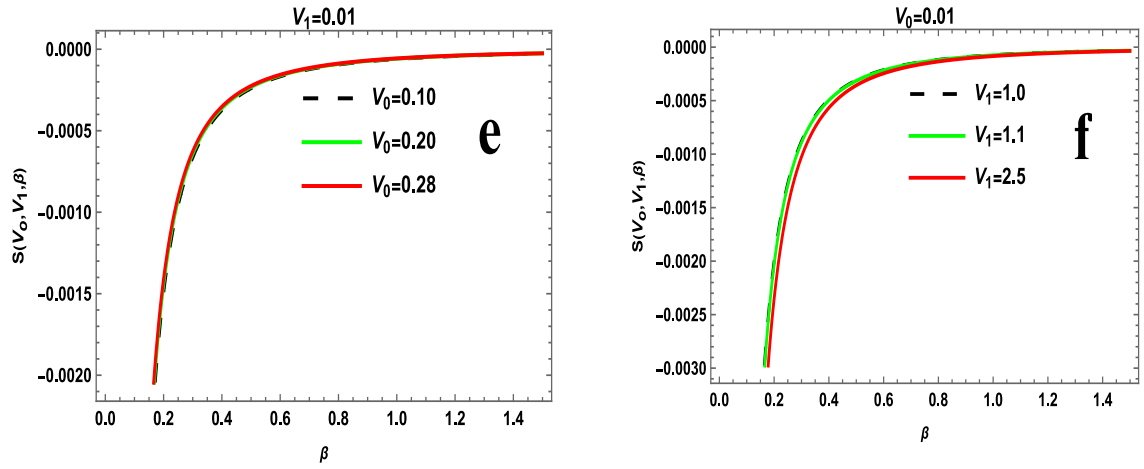

Figure 7: The Plot of Vibrational Entropy Under Varying Dimensional Potential Parameters

Figure 7 presents the molecular vibrational entropy across various conditions. In plot (a), the entropy exhibits a linear relationship as the dimensionless potential parameter and temperature parameter increase within the range of β=0.01–0.02, but shows a slight decline when β=0.022. Similarly, plot (b) demonstrates that as the temperature parameter β and dimensionless potential parameter V_0 increase together, the molecular vibrational entropy also rises. In plot (c), an increase in both dimensionless potential parameters V_0 and V_1 leads to higher molecular vibrational entropy. In contrast, plot (d) reveals that decreasing V_0 and V_1 results in a reduction in the molecular vibrational entropy. Lastly, plots (e) and (f) show the molecular vibrational entropy as a function of the temperature parameter, highlighting those simultaneous increases in V_0, V_1, and β contribute to an overall rise in the molecular vibrational entropy.

The molecular vibrational specific heat capacity can express

$$C_V = k_\beta \frac{\partial}{\partial \beta}(U) \tag{50}$$

$$P_{28} = \frac{P_{29}(P_{32}\sqrt{2\pi}P_{30})}{(\sqrt{\pi}(1+n+\sqrt{1+4(-\frac{f}{2b\delta^2}-\frac{af}{2b\delta^2}+\frac{2u}{\delta}+\lambda)}))} + P_{33} + P_{34} + P_{35}P_{36} + P_{37} + P_{38} + P_{39}P_{40}P_{41} + P_{42} \tag{51}$$

$$P_{29} = e^{\frac{1}{8}\sqrt{-\frac{af\beta\hbar^2}{b\mu}}\sqrt{\frac{\beta(-\frac{f}{4b\delta^2}+\frac{af}{4b\delta^2}+\frac{u}{\delta})^2\delta^2\hbar^2}{\mu}}-\frac{1}{2}\beta(\frac{(-\frac{f}{4b\delta^2}+\frac{af}{4b\delta^2}+\frac{u}{\delta})\delta^2\hbar^2}{2\mu}-\frac{af\delta^2\hbar^4}{8b\mu^2})} \tag{52}$$

$$P_{30} = ((P_{31} - \frac{af(1+n+\sqrt{1+4(-\frac{f}{2b\delta^2}-\frac{af}{2b\delta^2}+\frac{2u}{\delta}+\lambda)})^2\hbar^2}{16\sqrt{2}b\mu\sqrt{-\frac{af\beta\hbar^2}{b\mu}}} + \frac{(-\frac{f}{4b\delta^2}+\frac{af}{4b\delta^2}+\frac{u}{\delta})^2\delta^2\hbar^2}{2\sqrt{2}\mu\sqrt{\frac{\beta(-\frac{f}{4b\delta^2}+\frac{af}{4b\delta^2}+\frac{u}{\delta})^2\delta^2\hbar^2}{\mu}}}))$$

$$P_{31} = 2e^{\frac{1}{4}\sqrt{-\frac{af\beta\hbar^2}{b\mu}}\sqrt{\frac{\beta(-\frac{f}{4b\delta^2}+\frac{af}{4b\delta^2}+\frac{u}{\delta})^2\delta^2\hbar^2}{\mu}}-\frac{(\frac{(1+n+\sqrt{1+4(-\frac{f}{2b\delta^2}-\frac{af}{2b\delta^2}+\frac{2u}{\delta}+\lambda)})^2\sqrt{-\frac{af\beta\hbar^2}{b\mu}}}{8\sqrt{2}}+\frac{\sqrt{\frac{\beta(-\frac{f}{4b\delta^2}+\frac{af}{4b\delta^2}+\frac{u}{\delta})^2\delta^2\hbar^2}{\mu}}}{\sqrt{2}})^2}{(1+n+\sqrt{1+4(-\frac{f}{2b\delta^2}-\frac{af}{2b\delta^2}+\frac{2u}{\delta}+\lambda)})^2}} \tag{53}$$

$$P_{32} = \sqrt{-\frac{af\beta\hbar^2}{b\mu}}(\frac{1}{\sqrt{-\frac{af\beta\hbar^2}{b\mu}}}e^{-\frac{1}{8}\sqrt{-\frac{af\beta\hbar^2}{b\mu}}\sqrt{\frac{\beta(-\frac{f}{4b\delta^2}+\frac{af}{4b\delta^2}+\frac{u}{\delta})^2\delta^2\hbar^2}{\mu}}+\frac{1}{2}\beta(\frac{(-\frac{f}{4b\delta^2}+\frac{af}{4b\delta^2}+\frac{u}{\delta})\delta^2\hbar^2}{2\mu}-\frac{af\delta^2\hbar^4}{8b\mu^2})} \tag{54}$$

$$P_{33} = \frac{1}{\sqrt{\pi}}2e^{-(\frac{(1+n+\sqrt{1+4(-\frac{f}{2b\delta^2}-\frac{af}{2b\delta^2}+\frac{2u}{\delta}+\lambda)})\sqrt{-\frac{af\beta\hbar^2}{b\mu}}}{8\sqrt{2}}-\frac{\sqrt{\frac{\beta(-\frac{f}{4b\delta^2}+\frac{af}{4b\delta^2}+\frac{u}{\delta})^2\delta^2\hbar^2}{\mu}}}{\sqrt{2}(1+n+\sqrt{1+4(-\frac{f}{2b\delta^2}-\frac{af}{2b\delta^2}+\frac{2u}{\delta}+\lambda)})})^2} \tag{55}$$

$$P_{34} = (-\frac{af(1+n+\sqrt{1+4(-\frac{f}{2b\delta^2}-\frac{af}{2b\delta^2}+\frac{2u}{\delta}+\lambda)})\hbar^2}{16\sqrt{2}b\mu\sqrt{-\frac{af\beta\hbar^2}{b\mu}}} - \frac{(-\frac{f}{4b\delta^2}+\frac{af}{4b\delta^2}+\frac{u}{\delta})^2\delta^2\hbar^2}{2\sqrt{2}(1+n+\sqrt{1+4(-\frac{f}{2b\delta^2}-\frac{af}{2b\delta^2}+\frac{2u}{\delta}+\lambda)})\mu\sqrt{\frac{\beta(-\frac{f}{4b\delta^2}+\frac{af}{4b\delta^2}+\frac{u}{\delta})^2\delta^2\hbar^2}{\mu}}}) \tag{56}$$

$$P_{35} = e^{\frac{1}{4}\sqrt{-\frac{af\beta\hbar^2}{b\mu}}\sqrt{\frac{\beta(-\frac{f}{4b\delta^2}+\frac{af}{4b\delta^2}+\frac{u}{\delta})^2\delta^2\hbar^2}{\mu}}}\left(\frac{(-\frac{f}{4b\delta^2}+\frac{af}{4b\delta^2}+\frac{u}{\delta})^2\delta^2\hbar^2\sqrt{-\frac{af\beta\hbar^2}{b\mu}}}{8\mu\sqrt{\frac{\beta(-\frac{f}{4b\delta^2}+\frac{af}{4b\delta^2}+\frac{u}{\delta})^2\delta^2\hbar^2}{\mu}}} - \frac{af\hbar^2\sqrt{\frac{\beta(-\frac{f}{4b\delta^2}+\frac{af}{4b\delta^2}+\frac{u}{\delta})^2\delta^2\hbar^2}{\mu}}}{8b\mu\sqrt{-\frac{af\beta\hbar^2}{b\mu}}}\right) \quad (57)$$

$$P_{36} = (-1 + \mathrm{Erf}[\frac{\frac{(1+n+\sqrt{1+4(-\frac{f}{2b\delta^2}-\frac{af}{2b\delta^2}+\frac{2u}{\delta}+\lambda)})^2\sqrt{-\frac{af\beta\hbar^2}{b\mu}}}{8\sqrt{2}}+\frac{\sqrt{\frac{\beta(-\frac{f}{4b\delta^2}+\frac{af}{4b\delta^2}+\frac{u}{\delta})^2\delta^2\hbar^2}{\mu}}}{\sqrt{2}}}{1+n+\sqrt{1+4(-\frac{f}{2b\delta^2}-\frac{af}{2b\delta^2}+\frac{2u}{\delta}+\lambda)}}]) \quad (58)$$

$$P_{37} = \frac{1}{b\mu(-\frac{af\beta\hbar^2}{b\mu})^{3/2}} a e^{-\frac{1}{8}\sqrt{-\frac{af\beta\hbar^2}{b\mu}}\sqrt{\frac{\beta(-\frac{f}{4b\delta^2}+\frac{af}{4b\delta^2}+\frac{u}{\delta})^2\delta^2\hbar^2}{\mu}}+\frac{1}{2}\beta(\frac{(-\frac{f}{4b\delta^2}+\frac{af}{4b\delta^2}+\frac{u}{\delta})\delta^2\hbar^2}{2\mu}-\frac{af\delta^2\hbar^4}{8b\mu^2})} f\sqrt{\frac{\pi}{2}}\hbar^2(1 +$$

$$e^{\frac{1}{4}\sqrt{-\frac{af\beta\hbar^2}{b\mu}}\sqrt{\frac{\beta(-\frac{f}{4b\delta^2}+\frac{af}{4b\delta^2}+\frac{u}{\delta})^2\delta^2\hbar^2}{\mu}}}(-1 + \mathrm{Erf}[\frac{\frac{(1+n+\sqrt{1+4(-\frac{f}{2b\delta^2}-\frac{af}{2b\delta^2}+\frac{2u}{\delta}+\lambda)})^2\sqrt{-\frac{af\beta\hbar^2}{b\mu}}}{8\sqrt{2}}+\frac{\sqrt{\frac{\beta(-\frac{f}{4b\delta^2}+\frac{af}{4b\delta^2}+\frac{u}{\delta})^2\delta^2\hbar^2}{\mu}}}{\sqrt{2}}}{1+n+\sqrt{1+4(-\frac{f}{2b\delta^2}-\frac{af}{2b\delta^2}+\frac{2u}{\delta}+\lambda)}}]) \quad (59)$$

$$P_{38} = \mathrm{Erf}[\frac{(1+n+\sqrt{1+4(-\frac{f}{2b\delta^2}-\frac{af}{2b\delta^2}+\frac{2u}{\delta}+\lambda)})\sqrt{-\frac{af\beta\hbar^2}{b\mu}}}{8\sqrt{2}} - \frac{\sqrt{\frac{\beta(-\frac{f}{4b\delta^2}+\frac{af}{4b\delta^2}+\frac{u}{\delta})^2\delta^2\hbar^2}{\mu}}}{\sqrt{2}(1+n+\sqrt{1+4(-\frac{f}{2b\delta^2}-\frac{af}{2b\delta^2}+\frac{2u}{\delta}+\lambda)})}] \quad (60)$$

$$P_{39} = \frac{1}{\sqrt{-\frac{af\beta\hbar^2}{b\mu}}} e^{-\frac{1}{8}\sqrt{-\frac{af\beta\hbar^2}{b\mu}}\sqrt{\frac{\beta(-\frac{f}{4b\delta^2}+\frac{af}{4b\delta^2}+\frac{u}{\delta})^2\delta^2\hbar^2}{\mu}}+\frac{1}{2}\beta(\frac{(-\frac{f}{4b\delta^2}+\frac{af}{4b\delta^2}+\frac{u}{\delta})\delta^2\hbar^2}{2\mu}-\frac{af\delta^2\hbar^4}{8b\mu^2})}\sqrt{2\pi} \quad (61)$$

$$P_{40} = (-\frac{(-\frac{f}{4b\delta^2}+\frac{af}{4b\delta^2}+\frac{u}{\delta})^2\delta^2\hbar^2\sqrt{-\frac{af\beta\hbar^2}{b\mu}}}{16\mu\sqrt{\frac{\beta(-\frac{f}{4b\delta^2}+\frac{af}{4b\delta^2}+\frac{u}{\delta})^2\delta^2\hbar^2}{\mu}}} + \frac{af\hbar^2\sqrt{\frac{\beta(-\frac{f}{4b\delta^2}+\frac{af}{4b\delta^2}+\frac{u}{\delta})^2\delta^2\hbar^2}{\mu}}}{16b\mu\sqrt{-\frac{af\beta\hbar^2}{b\mu}}} + \frac{1}{2}(\frac{(-\frac{f}{4b\delta^2}+\frac{af}{4b\delta^2}+\frac{u}{\delta})\delta^2\hbar^2}{2\mu} - \frac{af\delta^2\hbar^4}{8b\mu^2})) \quad (62)$$

$$P_{41} = (1 + e^{\frac{1}{4}\sqrt{-\frac{af\beta\hbar^2}{b\mu}}\sqrt{\frac{\beta(-\frac{f}{4b\delta^2}+\frac{af}{4b\delta^2}+\frac{u}{\delta})^2\delta^2\hbar^2}{\mu}}}(-1 + \mathrm{Erf}[\frac{\frac{(1+n+\sqrt{1+4(-\frac{f}{2b\delta^2}-\frac{af}{2b\delta^2}+\frac{2u}{\delta}+\lambda)})^2\sqrt{-\frac{af\beta\hbar^2}{b\mu}}}{8\sqrt{2}}+\frac{\sqrt{\frac{\beta(-\frac{f}{4b\delta^2}+\frac{af}{4b\delta^2}+\frac{u}{\delta})^2\delta^2\hbar^2}{\mu}}}{\sqrt{2}}}{1+n+\sqrt{1+4(-\frac{f}{2b\delta^2}-\frac{af}{2b\delta^2}+\frac{2u}{\delta}+\lambda)}}]) \quad (63)$$

$$P_{42} = \mathrm{Erf}[\frac{(1+n+\sqrt{1+4(-\frac{f}{2b\delta^2}-\frac{af}{2b\delta^2}+\frac{2u}{\delta}+\lambda)})\sqrt{-\frac{af\beta\hbar^2}{b\mu}}}{8\sqrt{2}} - \frac{\sqrt{\frac{\beta(-\frac{f}{4b\delta^2}+\frac{af}{4b\delta^2}+\frac{u}{\delta})^2\delta^2\hbar^2}{\mu}}}{\sqrt{2}(1+n+\sqrt{1+4(-\frac{f}{2b\delta^2}-\frac{af}{2b\delta^2}+\frac{2u}{\delta}+\lambda)})}]))\mathrm{Log}[\beta] \quad (64)$$

$$= (\sqrt{2\pi}(1 + e^{\frac{1}{4}\sqrt{-\frac{af\beta\hbar^2}{b\mu}}\sqrt{\frac{\beta(-\frac{f}{4b\delta^2}+\frac{af}{4b\delta^2}+\frac{u}{\delta})^2\delta^2\hbar^2}{\mu}}}(-1$$

$$+ \mathrm{Erf}[P_{43}\frac{\frac{(1+n+\sqrt{1+4(-\frac{f}{2b\delta^2}-\frac{af}{2b\delta^2}+\frac{2u}{\delta}+\lambda)})^2\sqrt{-\frac{af\beta\hbar^2}{b\mu}}}{8\sqrt{2}}+\frac{\sqrt{\frac{\beta(-\frac{f}{4b\delta^2}+\frac{af}{4b\delta^2}+\frac{u}{\delta})^2\delta^2\hbar^2}{\mu}}}{\sqrt{2}}}{1+n+\sqrt{1+4(-\frac{f}{2b\delta^2}-\frac{af}{2b\delta^2}+\frac{2u}{\delta}+\lambda)}}])$$

$$P_{44} = \mathrm{Erf}[\frac{(1+n+\sqrt{1+4(-\frac{f}{2b\delta^2}-\frac{af}{2b\delta^2}+\frac{2u}{\delta}+\lambda)})\sqrt{-\frac{af\beta\hbar^2}{b\mu}}}{8\sqrt{2}} - \frac{\sqrt{\frac{\beta(-\frac{f}{4b\delta^2}+\frac{af}{4b\delta^2}+\frac{u}{\delta})^2\delta^2\hbar^2}{\mu}}}{\sqrt{2}(1+n+\sqrt{1+4(-\frac{f}{2b\delta^2}-\frac{af}{2b\delta^2}+\frac{2u}{\delta}+\lambda)})}] \quad (65)$$

$$P_{45} = \text{Log}[\frac{1}{\sqrt{-\frac{af\beta\hbar^2}{b\mu}}} e^{-\frac{1}{8}\sqrt{-\frac{af\beta\hbar^2}{b\mu}}\sqrt{\frac{\beta(-\frac{f}{4b\delta^2}+\frac{af}{4b\delta^2}+\frac{u}{\delta})^2\delta^2\hbar^2}{\mu}}+\frac{1}{2}\beta(\frac{(-\frac{f}{4b\delta^2}+\frac{af}{4b\delta^2}+\frac{u}{\delta})\delta^2\hbar^2}{2\mu}-\frac{af\delta^2\hbar^4}{8b\mu^2})}\sqrt{2\pi}(1 +$$

$$e^{\frac{1}{4}\sqrt{-\frac{af\beta\hbar^2}{b\mu}}\sqrt{\frac{\beta(-\frac{f}{4b\delta^2}+\frac{af}{4b\delta^2}+\frac{u}{\delta})^2\delta^2\hbar^2}{\mu}}}(-1 + \text{Erf}[\frac{\frac{(1+n+\sqrt{1+4(-\frac{f}{2b\delta^2}-\frac{af}{2b\delta^2}+\frac{2u}{\delta}+\lambda)})^2\sqrt{-\frac{af\beta\hbar^2}{b\mu}}}{8\sqrt{2}}+\frac{\sqrt{\frac{\beta(-\frac{f}{4b\delta^2}+\frac{af}{4b\delta^2}+\frac{u}{\delta})^2\delta^2\hbar^2}{\mu}}}{\sqrt{2}}}{1+n+\sqrt{1+4(-\frac{f}{2b\delta^2}-\frac{af}{2b\delta^2}+\frac{2u}{\delta}+\lambda)}}]) +$$

$$\text{Erf}[\frac{(1+n+\sqrt{1+4(-\frac{f}{2b\delta^2}-\frac{af}{2b\delta^2}+\frac{2u}{\delta}+\lambda)})\sqrt{-\frac{af\beta\hbar^2}{b\mu}}}{8\sqrt{2}} - \frac{\sqrt{\frac{\beta(-\frac{f}{4b\delta^2}+\frac{af}{4b\delta^2}+\frac{u}{\delta})^2\delta^2\hbar^2}{\mu}}}{\sqrt{2}(1+n+\sqrt{1+4(-\frac{f}{2b\delta^2}-\frac{af}{2b\delta^2}+\frac{2u}{\delta}+\lambda)})}])]^2$$

$$(\beta\text{Log}[\frac{1}{\sqrt{-\frac{af\beta\hbar^2}{b\mu}}} e^{-\frac{1}{8}\sqrt{-\frac{af\beta\hbar^2}{b\mu}}\sqrt{\frac{\beta(-\frac{f}{4b\delta^2}+\frac{af}{4b\delta^2}+\frac{u}{\delta})^2\delta^2\hbar^2}{\mu}}+\frac{1}{2}\beta(\frac{(-\frac{f}{4b\delta^2}+\frac{af}{4b\delta^2}+\frac{u}{\delta})\delta^2\hbar^2}{2\mu}-\frac{af\delta^2\hbar^4}{8b\mu^2})} \quad (66)$$

$$P_{46} = \frac{1}{(\sqrt{2\pi}P_{47}-\frac{\sqrt{\frac{\beta(-\frac{f}{4b\delta^2}+\frac{af}{4b\delta^2}+\frac{u}{\delta})^2\delta^2\hbar^2}{\mu}}}{\sqrt{2}(1+n+\sqrt{1+4(-\frac{f}{2b\delta^2}-\frac{af}{2b\delta^2}+\frac{2u}{\delta}+\lambda)})})k_\beta} \quad (67)$$

$$P_{47} = (-1 + \text{Erf}[\frac{\frac{(1+n+\sqrt{1+4(-\frac{f}{2b\delta^2}-\frac{af}{2b\delta^2}+\frac{2u}{\delta}+\lambda)})^2\sqrt{-\frac{af\beta\hbar^2}{b\mu}}}{8\sqrt{2}}+\frac{\sqrt{\frac{\beta(-\frac{f}{4b\delta^2}+\frac{af}{4b\delta^2}+\frac{u}{\delta})^2\delta^2\hbar^2}{\mu}}}{\sqrt{2}}}{1+n+\sqrt{1+4(-\frac{f}{2b\delta^2}-\frac{af}{2b\delta^2}+\frac{2u}{\delta}+\lambda)}}](1 + e^{\frac{1}{4}\sqrt{-\frac{af\beta\hbar^2}{b\mu}}\sqrt{\frac{\beta(-\frac{f}{4b\delta^2}+\frac{af}{4b\delta^2}+\frac{u}{\delta})^2\delta^2\hbar^2}{\mu}}}) +$$

$$\text{Erf}[\frac{(1+n+\sqrt{1+4(-\frac{f}{2b\delta^2}-\frac{af}{2b\delta^2}+\frac{2u}{\delta}+\lambda)})\sqrt{-\frac{af\beta\hbar^2}{b\mu}}}{8\sqrt{2}} \quad (68)$$

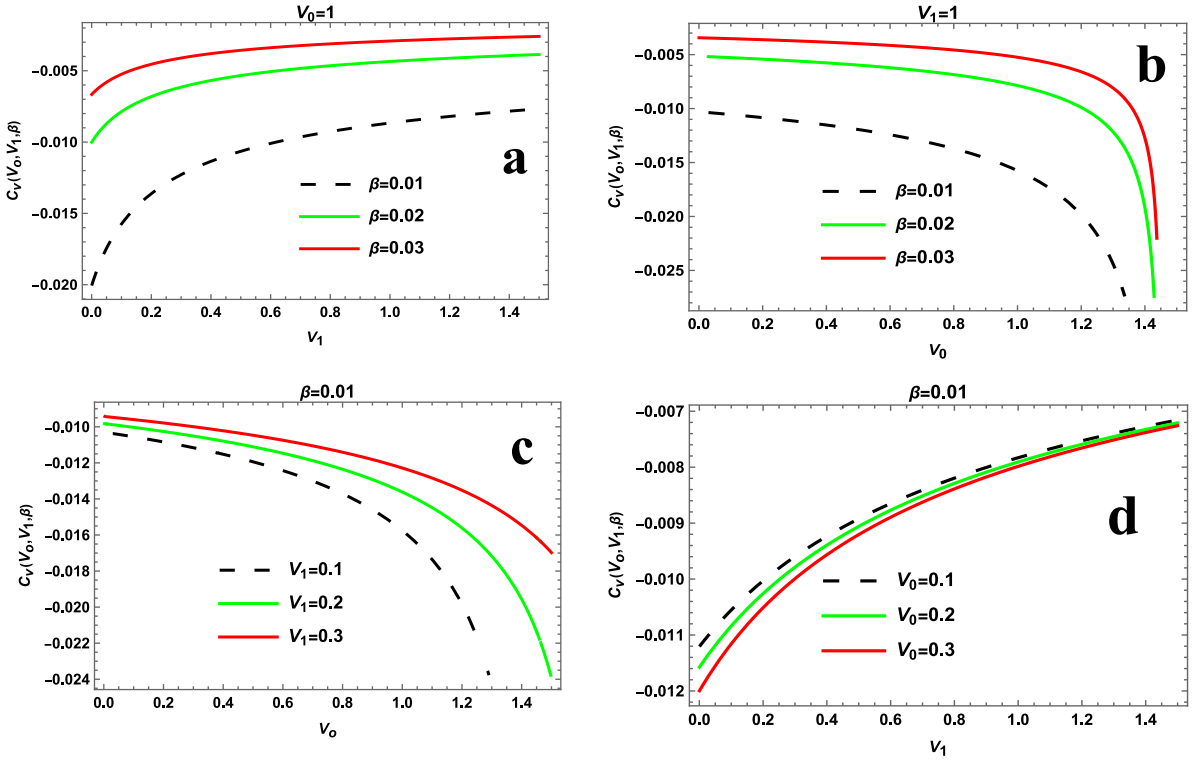

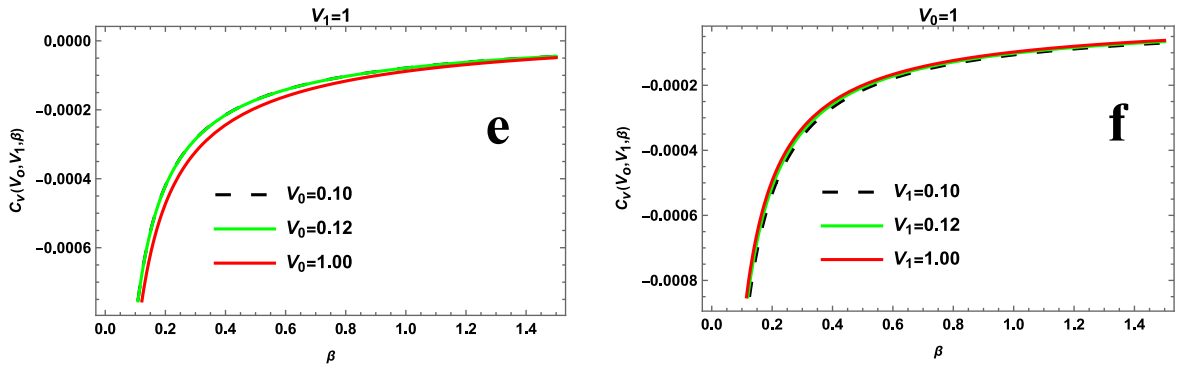

Figure 8: The plot of vibrational entropy under varying dimensionless potential parameters.

Figure 8 depicts the molecular vibrational specific heat capacity as a function of various parameters. In plot (a), increasing the temperature parameter in the range of β = 0.01 to 0.02 causes an increase in the specific heat capacity, while at β = 0.03, the capacity decreases. Plot (b) demonstrates that a simultaneous increase in the temperature parameter and the dimensionless potential parameter V_0 leads to a higher specific heat capacity. Plot (c) reveals that an increase in both dimensionless potential parameters, V_0 and V_1, results in a reduction of the specific heat capacity. In contrast, plot (d) shows that an increase in the dimensionless potential parameter alone leads to an increase in the specific heat capacity. Plots (e) and (d) also plot the molecular vibrational specific heat capacity against the temperature parameter, further confirming that an increase in the dimensionless potential parameter results in a higher specific heat capacity.

Magnetisation and magnetic susceptibility at Zero Temperature can be writen as

$$\mathrm{M_{nm}} = -\frac{\partial(\mathrm{E_{nm}})}{\partial V_0} \tag{69}$$

$$\boldsymbol{X_M} = \frac{\partial \mathrm{M_{nm}}}{\partial V_0} \tag{70}$$

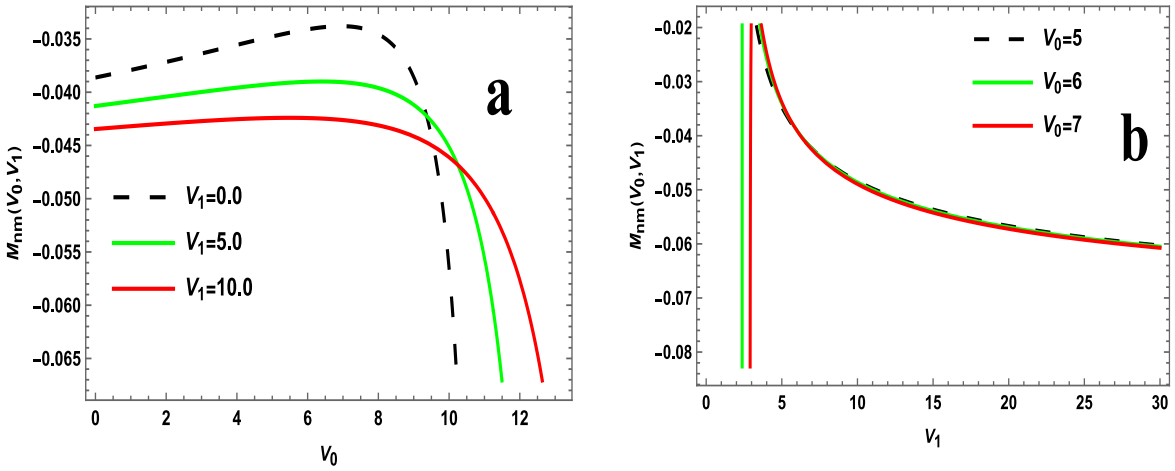

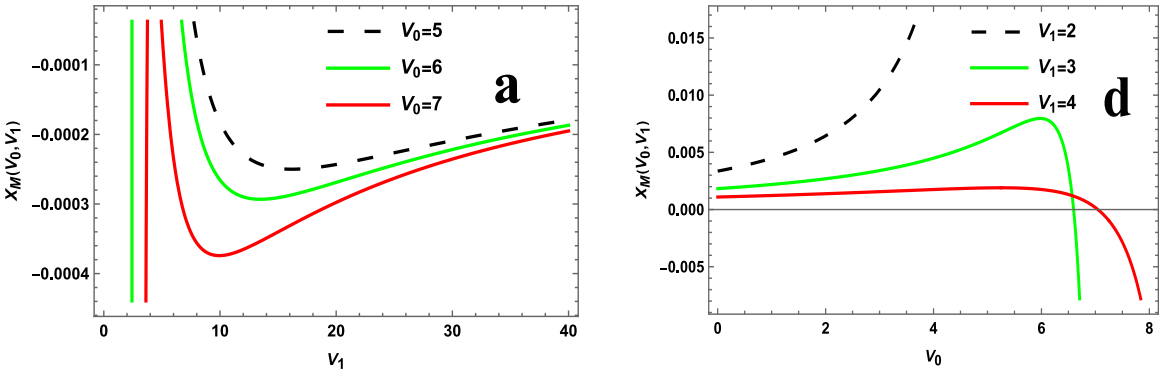

Figure 9: The Plot Magnetisation at Zero Under Varying Dimensionless Potential Parameters

Figure 9 displays the plot of magnetization at zero temperature for varying dimensionless potential parameters. Each subplot illustrates how magnetization and magnetic susceptibility depend on the dimensionless potential parameters V_0 and V_1. In plot (a), the magnetization $M_{mm}(V_0, V_1)$ is shown as a function of V_0 for fixed values of V_1. When V_1=0, magnetization initially increases with V_0 before dropping sharply at larger V_0. For higher values of V_1 (e.g., 5 and 10), magnetization increases more slowly and then also decreases at higher V_0. This indicates that while magnetization is enhanced at small V_0, it is suppressed at larger V_0, with the suppression becoming more pronounced as V_1 increases.

In plot (b), magnetization is plotted against V_1 for various fixed V_0 values. The magnetization decreases rapidly with increasing V_1, and the curves nearly coincide, suggesting minimal dependence on V_0. Plot (c) presents magnetic susceptibility $\chi_m(V_0, V_1)$ versus V_1 for different V_0 values. All curves display a pronounced dip at low V_1, followed by a gradual recovery as V_1 grows. Overall, the magnitude of susceptibility remains negative, indicating a diamagnetic response. In plot (d), the susceptibility initially rises with increasing V_1, peaks, and then decreases at higher V_1. Notably, the peak location shifts to lower V_1 values as V_0 increases.

CONCLUSION

This study employs partition function methods derived from the non-relativistic Schrödinger equation to determine thermodynamic properties, emphasizing how dimensionless potential parameters influence the quantum energy spectrum. It finds that energy eigenvalues are highly sensitive to these potential parameters, with the dimensionless parameter λ playing a crucial role in defining the quantum states. Using the calculated energy spectrum, thermodynamic quantities like magnetization and magnetic susceptibility are derived, revealing that magnetization generally decreases with increasing potential parameter V_0 and temperature, but rises with V_1 and higher temperatures. Magnetic susceptibility shows varying trends—diminishing with higher temperature and V_0, increasing with V_1, and saturating at high parameter ranges. Molecular vibrational energy and free energy demonstrate complex dependencies on temperature and potential parameters, with vibrational energy either decreasing or increasing depending on parameter ranges, and vibrational free energy consistently declining when both parameters increase. Entropy grows with higher potential and temperature parameters, reflecting an increase in system disorder, while specific heat capacity varies depending on the conditions, highlighting quantum transitions. At zero temperature, magnetization and magnetic susceptibility exhibit a delicate interplay between $V_0$and V_1, with magnetization showing initial growth and subsequent suppression, and susceptibility displaying characteristic diamagnetic features. The findings underscore the efficacy of using partition function approaches to connect quantum mechanical details to macroscopic thermodynamic behaviour, offering valuable insights for condensed matter physics and materials research.

REFERENCES

Abu-Shady, M., & Khokha, E. M. (2023). A precise estimation for vibrational energies of diatomic molecules using the improved Rosen–Morse potential. *Scientific Reports*, *13*(1), 11578.

Ding, Y., & Wang, Z. Q. (2011). Bound states of nonlinear Schrödinger equations with magnetic fields. *Annali di Matematica Pura ed Applicata*, *190*(3), 427-451.

Dong, S. H. (2000). Exact solutions of the two-dimensional Schrödinger equation with certain central potentials. *International Journal of Theoretical Physics*, *39*, 1119-1128.

Edet, C. O., Amadi, P. O., Onyeaju, M. C., Okorie, U. S., Sever, R., Rampho, G. J., ... & Ikot, A. N. (2021). Thermal properties and magnetic susceptibility of

Hellmann potential in Aharonov–Bohm (AB) flux and magnetic fields at zero and finite temperatures. *Journal of Low Temperature Physics*, *202*, 83-105.

Ettah, E. (2021). The Schrödinger Equation with Deng-Fan-Eckart Potential (DFEP): Nikiforov-Uvarov-Functional Analysis (NUFA) Method. *European Journal of Applied Physics*, *3*(5), 58-62.

Ikot, A. N., Okorie, U. S., Amadi, P. O., Edet, C. O., Rampho, G. J., & Sever, R. (2021). The Nikiforov–Uvarov-Functional Analysis (NUFA) Method: A new approach for solving exponential-type potentials. *Few-Body Systems*, *62*, 1-16.

Jia, C. S., Diao, Y. F., Liu, X. J., Wang, P. Q., Liu, J. Y., & Zhang, G. D. (2012). Equivalence of the Wei potential model and Tietz potential model for diatomic molecules. *The Journal of chemical physics*, *137*(1).

Lublinsky, M., & Mulian, Y. (2017). High Energy QCD at NLO: from light-cone wave function to JIMWLK evolution. *Journal of High Energy Physics*, *2017*(5), 1-80.

Manga, P. J., Buteh, S. D., Maina, M., Amusat, R. O., Teru, P. B., Hashimu, M. U., & John, D. S. (2023). Solutions of Schrödinger equation based on Modified Exponential Screened Plus Yukawa Potential (MESPYP) within the frame of parametric Nikiforov-Uvarov method. *Dutse Journal of Pure and Applied Sciences*, *9*(3b), 144-154.

Manga, P. J., Likta, E. W., & Teru, P. B. (2021). Comparative Study on Charged and Neutral Pion-Nucleon Coupling Constants Using Yukawa Potential Model. *FUDMA JOURNAL OF SCIENCES*, *5*(4), 167-173.

Mulian, Y. (2025). The Magnus expansion for non-Hermitian Hamiltonians. *arXiv preprint arXiv:2505.09559*.

Onate, C., Okon, I. B., Onyeaju, M. C., & Antia, A. D. (2022). Approximate solutions of the Schrodinger Equation for a Momentum-Dependent potential. *Journal of the Nigerian Society of Physical Sciences*, 242-250.

Reiss, H. R. (1980). Effect of an intense electromagnetic field on a weakly bound system. *Physical Review A*, *22*(5), 1786.

Umirzakov, I. (2019). Incorrectness of analytical solution of Schrodinger equation for diatomic molecule with shifted Tietz-Wei potential. *arXiv preprint arXiv:1902.04977*.